SPACE
SCIENCES
LABORATORY

FINAL REPORT

NASA Grant NGR 05-003-414

PETROGRAPHIC AND CRYSTALLOGRAPHIC STUDY OF
SILICATE MINERALS IN LUNAR ROCKS

Period of Performance

February 1, 1971 - January 31, 1972

Principal Investigators

Prof. I. S. E. Carmichael

Prof. F. J. Turner

Prof. H.-R. Wenk

March 25, 1974

Space Sciences Laboratory Series 15 Issue 17

UNIVERSITY OF CALIFORNIA, BERKELEY

FINAL REPORT

NASA Grant NGR 05-003-414

PETROGRAPHIC AND CRYSTALLOGRAPHIC STUDY OF
SILICATE MINERALS IN LUNAR ROCKS

Period of Performance
February 1, 1971 - January 31, 1972

Principal Investigators
Prof. I. S. E. Carmichael
Prof. F. J. Turner
Prof. H.-R. Wenk

March 25, 1974
Space Sciences Laboratory Series 15 Issue 17

Space Sciences Laboratory
University of California
Berkeley, California 94720

FINAL REPORT

NASA Grant NGR 05-003-414

Petrographic and Crystallographic Study of

Silicate Minerals in Lunar Rocks

Period of Performance
2/1/71 - 1/31/72

Principal Investigators

Prof. I. S. E. Carmichael

Prof. F. J. Turner

Prof. H.-R. Wenk

March 25, 1974

Series 15 Issue 17

Table of Contents

Lunar bytownite from sample 12032,44

H.-R. WENK and G. L. NORD

Department of Geology and Geophysics, University of California at Berkeley
Berkeley, California 94720

Abstract—Optical U-stage measurements, chemical microprobe data, and X-ray precession photographs of a bytownite twin group from rock 12032,44 are compared. Sharp but weak b and no c-reflections were observed for this An89 bytownite indicating a partly disordered structure. Euler angles, used to characterize the orientation of the optical indicatrix, compare better with values for plutonic than for volcanic plagioclase. This indicates that structural and optical properties cannot be directly correlated.

INTRODUCTION

THIS PAPER REPORTS optical, chemical, and structural data for a group of plagioclase crystals twinned after various laws. The group of crystals was a fragment in the fines of specimen 12032,44 from Oceanus Procellarum. Rock 12032,44 belongs to WOOD's (1971) group of gabbroic anorthosites or norites which may come from the lunar highlands. A thin section, prepared from the specimen, which is 2 mm in size (Fig. 1a), was cut perpendicular to [100] in order to facilitate measurements of twin lamellae and cleavage. Optical measurements were obtained on a Leitz U-stage for locations indicated in Fig. 1a. The section was then polished and chemical analyses were done using an ARL microprobe. Finally, two crystal fragments (X and R in Fig. 1a) were picked from the thin section for X-ray analysis on a precession camera (X) and for determination of the refractive index on a spindle stage (N). All measurements were made on the same group of crystals and are therefore directly comparable.

CHEMICAL COMPOSITION

As both structure and optical properties of plagioclase are sensitive to variations in chemical composition and conditions during the formation of the crystal, it is essential to have accurate chemical analyses; 77 spot analyses have been done over the whole group of crystals. Representative results are shown in Fig. 1b and Table 1. The plagioclase is a bytownite, An 85–90, the rim slightly more sodic than the center. Fe is the only other element which we have found to be relatively abundant. It is assumed to be in the ferrous oxidation state and evidence from Mössbauer spectra indicates that it occurs both in the tetrahedral and calcium sites (APPLEMAN *et al.*, 1971; HAFNER and VIRGO, 1971).

OPTICAL ANALYSIS

The crystals shown in Fig. 1a form a multiple twin group. They appear undeformed but the composition planes are slightly curved. U-stage measurements with a Leitz UM3 20X objective have been done in areas A and B of the specimen (Fig. 1a). Independent raw measurements are shown in Figs. 1c and d. There is some scatter

Fig. 1. (a) Photomicrograph of the twin individuals in specimen 12032,44 which have been used in this analysis. Locations of optical and X-ray measurements are indicated (Zeiss Ultraphot 111). (b) Map of the crystals, giving chemical composition (An content in mole %). (c–f) Stereograms showing the orientation of the optical indicatrix and the construction of the Euler angles in area A (c, e) and B (d, f). Same orientation as Fig. 1a, upper hemisphere. (c, d) Raw U-stage measurements, A, B = optic axes. (e, f) Construction of Euler I angles. $\odot = \alpha$, $\div = \beta$, $\triangle = \gamma$, RT = Roc Tourné twin axis $\perp$ [001] in (010).

Table 1. Chemical analyses for lunar bytownite 12032,44 (determined with an ARL microprobe).

	Average of 77 spots over entire specimen	Area A	Area B	Single Crystal ×	Stoichiometric An$_{89}$ (for comparison)
			weight %		
SiO$_2$	46.8	46.6	46.3	46.5	46.0
Al$_2$O$_3$	33.2	33.5	33.4	33.5	34.8
CaO	17.7	17.9	17.9	17.7	17.9
K$_2$O	0.01	0.01	0.01	0.01	
Na$_2$O	1.44	1.32	1.32	1.37	1.30
SrO	0.03	0.03	0.03	0.03	
FeO	0.34	0.33	0.31	0.42	
TOTAL*	99.5	99.7	99.3	99.5	100.0
			Mole %		
An	88.8$_8$	89.7$_0$	89.7$_6$	89.1$_3$	89.0
Or	0.02	0.03	0.03	0.03	0.0
Ab	11.1$_0$	10.2$_7$	10.2$_1$	10.8$_4$	11.0

* Low totals due to small errors in the determinations of Al and Si.

in the data which we attribute partly to difficulties in measuring these relatively small crystals, and also to the limits of resolution of the U-stage. A numerical average of the measurements has been used in the subsequent derivation of the Euler angles (BURRI, 1956) which are used to characterize the orientation of the optical indicatrix. This average appears to be reliable: optical directions were mutually perpendicular within ±1 deg, the error triangle in the construction of the twin axis was less than 2 deg. Constructed and calculated composition planes agree within 2 deg. The cleavage is poorly developed and has not been used in the analysis. Euler 1 angles were constructed in group A from optical directions of a complex Albite (1–2)-Roc Tourné (1–3)—Carlsbad (2–3) twin group; constructed and measured poles to (010) were averaged (Fig. 1e). In group B the Euler I angles were derived from a Roc Tourné twin (4–5) and the measured composition plane (010) (Fig. 1f). The relationship between crystals 3 and 4 is an irrational intergrowth without a twin axis, although the composition plane is a well-developed face approximately parallel to (010).

Euler I angles determined on five crystals are listed on Table 2. The measurements on 2A are least reliable as the thin lamellae overlap partly during tilting and these measurements have been omitted in the calculation of an average. From the averaged Euler I angles and from $2V\gamma = 99\frac{1}{2}$ deg, additional positional angles have been calculated:

Euler II: R = 118.0 deg, I = 91.5 deg, Lα = 53.5 deg, L$_A$ = 13.3 deg, L$_B$ = 93.8 deg
Euler III: D = 29.1 deg, N = 53.5 deg, Aα = 91.8 deg
Goldschmidt ([001] normal):

ϕ	206.0 deg	298.0 deg	29.1 deg	207.7 deg	49.5 deg
	α	,β	,γ	,A	,B
ρ	36.5 deg	88.5 deg	53.5 deg	76.7 deg	4.1 deg

In Fig. 2, Φ and Ψ of the lunar bytownite (An 89%) are compared with the curves of BURRI *et al.* (1967) and with the volcanic, An 85% bytownite from Cape Parry (WENK *et al.*, 1968). There is a significant difference in the orientation of the optical indicatrix which suggests that the lunar bytownite may have formed under plutonic rather than under volcanic conditions. The values are intermediate between bytownites from mafic intrusives such as the Bushfeld complex (An 87.5, BURRI *et al.*, 1967) and Åkero in Sweden (An 90.9, NIKITIN, 1933). These data for a plagioclase from 12032,44 are different from the observations of BANCROFT *et al.* (1971) for plagioclase from basaltic rocks 12051, 12052. They describe volcanic optics but no data are presented which would permit a quantitative comparison. Bytownites and anorthites from meteorites were described as having plutonic optical properties (ULBRICH, 1971).

Table 2. Euler I angles for lunar plagioclase from rock 12032,44.

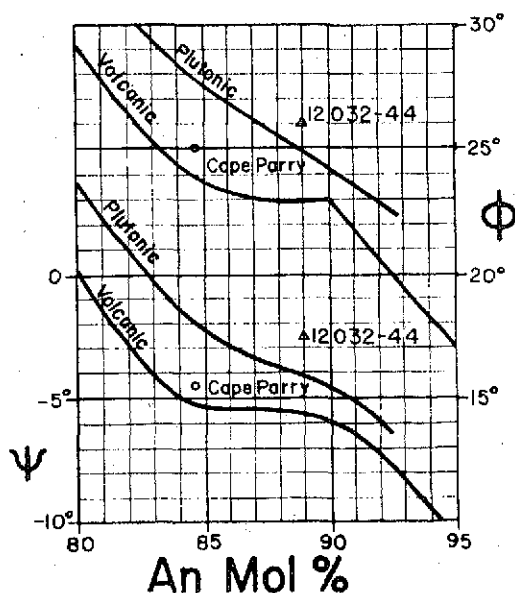|		Φ	Θ	Ψ	$2V_y$
Group A	1	26°	37°	−2°	
	2	22°	38¼°	−1°	98
	3	26°	36°	−3°	98
	5				100
Group B	4	26°	36°	−2°	101
	5	26°	36¼°	−3°	97
	2				101
Average		26°	36¼°	−2¼°	99¼

Fig. 2. Diagram of Euler angles Ψ and Φ as a function of the An-content (after BURRI *et al.*, 1968). Lunar bytownite from 12032,44 and volcanic bytownite from Cape Parry (WENK *et al.*, 1969) are indicated.

Refractive indices were measured in fragment R on a spindle stage with oil immersion and Na-light. The small size of the specimen (only 0.02 mm thick) limited us to determinations of α' and γ' in (010).

$$\alpha': 1.576 \pm 0.001 \qquad \gamma': 1.583 \pm 0.001$$

STRUCTURE

X-ray single-crystal measurements have been done to determine lattice constants and presence or absence of reflections which are indicative of the structural state. Other investigators describe diffuse to sharp b and diffuse to very diffuse c reflections using X-ray and electron diffraction (APPLEMAN *et al.*, 1971; BANCROFT *et al.*, 1971; CHRISTIE *et al.*, 1971). An 850 hour precession *a* exposure (Fig. 3a) shows that this bytownite (fragment X, in Fig. 1a) has a body-centered anorthite structure with sharp b reflections. c-reflections were not observed even with long exposure times. c-reflections become diffuse with disorder and increasing albite content. Comparison of the lunar plagioclase with one of identical composition, an An 89 bytownite from a gabbro of the basal zone of the Stillwater complex, removes this ambiguity. The Stillwater bytownite 0kl photograph (Fig. 3b) shows sharp b and moderate but diffuse c-reflections. The apparent absence or extreme weakness of c-reflections in the lunar bytownite (Fig. 3a) indicates that it is more disordered than the terrestrial one. This differs from plagioclase from some lunar "basalts" which have a "low structural state" (APPLEMAN *et al.*, 1971, p. 8).

Lattice constants were determined from sets of precession photographs on the fragment X (Fig. 1a): $a_0 = 8.16 \text{ Å} \pm 0.01$; $b_0 = 12.89 \text{ Å} \pm 0.01$; $c_0 = 14.18 \text{ Å} \pm 0.01$; $\alpha = 93.53° \pm 0.1$; $\beta = 115.8° \pm 0.1$; $\gamma = 90.8° \pm 0.1$; $V = 1338.0 \text{ Å}^3$; $\gamma^* = 87.4° \pm 0.1$. They compare well with data given by APPLEMAN *et al.* (1971) but are inconclusive with respect to the structural state.
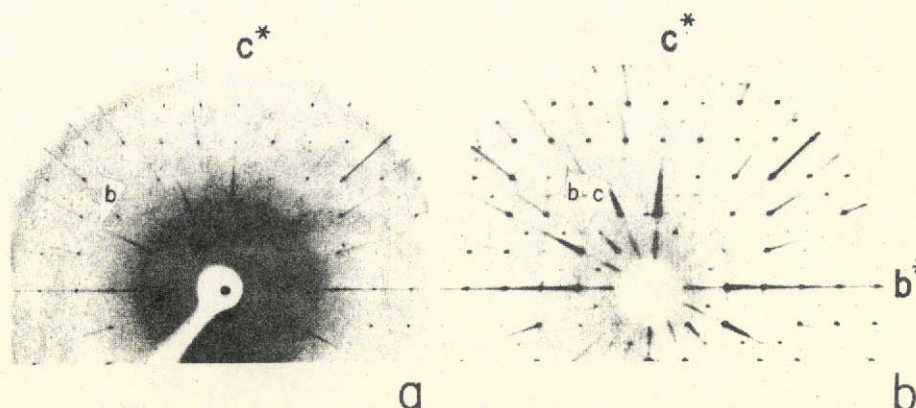

Fig. 3. Precession 0kl-photographs of bytownites. b* is horizontal. Mo radiation, Zr filter, b ($h + k$ odd, l odd), and c ($h + k$ even, l odd) reflections are indicated. (a) Lunar bytownite An 89, X (Fig. 1a), from 12032,44. 850-hour exposure. (Includes faint albite twin.) Note absence of c-reflections. (b) Bytownite An 89, from a gabbro of the Stillwater complex, 50-hour exposure. Note diffuse but moderately intensive c-reflections.

In the bytownite from 12032,44 optical measurements indicate plutonic properties whereas X-ray data indicate a partially disordered structure. It appears to be another case where "disordered" structure does not correspond to volcanic optics (cf. WENK, 1969). The relationship between optical and structural parameters is the subject of a current experimental investigation. It seems that there is no simple direct correlation between the two, although in most cases "volcanic optics" is found in feldspar with a disordered structure.

REFERENCES

APPLEMAN D. E., NISSEN H. U., STEWART D. B., CLARK J. R., DOWTY E., and HUEBNER J. S. (1971) Crystallographic studies of Apollo 11 and Apollo 12 plagioclase, tridymite, and cristobalite. Second Lunar Science Conference (unpublished proceedings).

BANCROFT G. M., BROWN M. G., GAY P., MUIR I. D., and WILLIAMS P. G. L. (1971) Mineralogical and petrographic investigation of some Apollo 12 samples. Second Lunar Science Conference (unpublished proceedings).

BURRI C. (1956) Charakterisierung der Plagioklasoptik durch drei Winkel und Neuentwurf des Stereogramms der optischen Orientierung für konstante Anorthit-Intervalle. *Schweiz. mineral. petrog. Mitt.* **36**, 539–592.

BURRI C., PARKER R. L., and WENK E. (1967) *Die optische Orientierung der Plagioklase.* Birkhäuser, Basel.

CHRISTIE J. M., FISHER R. M., GRIGGS D. T., HEUER A. H., LALLY J. S., and RADCLIFFE S. V. (1971) Comparative electron petrography of Apollo 11, Apollo 12, and terrestrial rocks. Second Lunar Science Conference (unpublished proceedings).

NIKITIN W. W. (1933) Korrekturen and Vervollständigungen der Diagramme zur Bestimmung der Feldspate nach Fedorows Methode. *Mineral. petrog. Mitt. Tscherm.* [N. F.] **44**, 117–167.

ULBRICH M. (1971) Systematics of eucrites and howardite meteorites and a petrographic study of representative individual eucrites. M.A. thesis, University of California, Berkeley.

VIRGO D., HAFNER S. S., and WARBURTON D. (1971) Cation distribution studies in clinopyroxenes, olivines, and feldspars using Mössbauer spectroscopy of ^{57}Fe. Second Lunar Science Conference (unpublished proceedings).

WENK E., WENK H.-R., and SCHWANDER H. (1968) Bytownite from Cape Parry, East Greenland. *Amer. Mineral.* **53**, 1759–1764.

WENK H.-R. (1969) Annealing of oligoclase at high pressure. *Amer. Mineral.* **54**, 95–100.

WOOD J. A., MARVIN V., REID J. B., TAYLOR G. J., BOWER J. F., POWELL B. N., and DICKEY J. S., JR. (1971) Relative proportions of rock types, and nature of the light-colored lithic fragments in Apollo 12 soil samples. Second Lunar Science Conference (unpublished proceedings).

Lunar plagioclase: A mineralogical study

H.-R. WENK and M. ULBRICH

Department of Geology and Geophysics
and Space Sciences Laboratory,
University of California at Berkeley

and

W. F. MÜLLER

Department of Materials Science and Engineering,
University of California at Berkeley

Abstract —Mineralogical properties of calcic plagioclase have been analyzed using U-stage, microprobe, x-ray precession cameras, and a 650 kV electron microscope. The orientation of the optical indicatrix in lunar and eucrite anorthites is described with Euler angles. All crystals, except one, show strong b- and diffuse c-reflections in precession photographs. In 10017, b-split-reflections have been found. Dark-field electron micrographs of 14310 anorthite show both large and small b-antiphase domains, and an exsolution structure in crystals that display b-split reflections in the diffractogram. Diffuseness of c-reflections in x-ray photographs and the inability to resolve c-domains in electronmicrographs in An 94 anorthite of 14310 indicate relatively rapid cooling of this rock compared to plutonic rocks.

INTRODUCTION

IT WAS THE PURPOSE OF this study to describe the properties of lunar plagioclase and to investigate, by comparison with appropriate terrestrial feldspars, whether the optics and structure of anorthite are indicative of the thermal history of the crystals. Documentation on anorthites is sparse; therefore, lunar rocks provide excellent material to study calcic plagioclase and these new data contribute to a better understanding of this important mineral series.

Techniques used include determination of optical properties on the universal stage, single crystal x-ray photography by the precession method, chemical microprobe analyses, and 650–kV transmission electron microscopy. Procedures are similar to those described by Wenk and Nord (1971). First, a polished thin section was prepared and examined on the petrographic microscope. U-stage measurements were made on several multiply twinned plagioclase crystals (preferentially twinned after albite and albite-Carlsbad laws). Then the chemical composition (Ca, Na, K) was determined on the same spots by microprobe. One crystal was picked either from the thin section or from the rock for x-ray study and later analyzed chemically. Electron microscope samples were prepared from thin sections using the ion thinning technique.

Most of our data were obtained on the only two available thin sections, 14310 (basalt) and 14319 (breccia). Fines were usually not satisfactory for this analysis. Some measurements have been done on small fragments of 10017, 12021, and 14162. The results reported apply only to these few specimens and not to lunar rocks in general.

PETROGRAPHY

Basalt 14310 (Fig. 1a) consists mainly of clear, inclusion-free crystals of calcic plagioclase (An 85–95), clinopyroxene ($2V_\gamma = 12$–$20°$), orthopyroxene ($2V_a = 72°$),
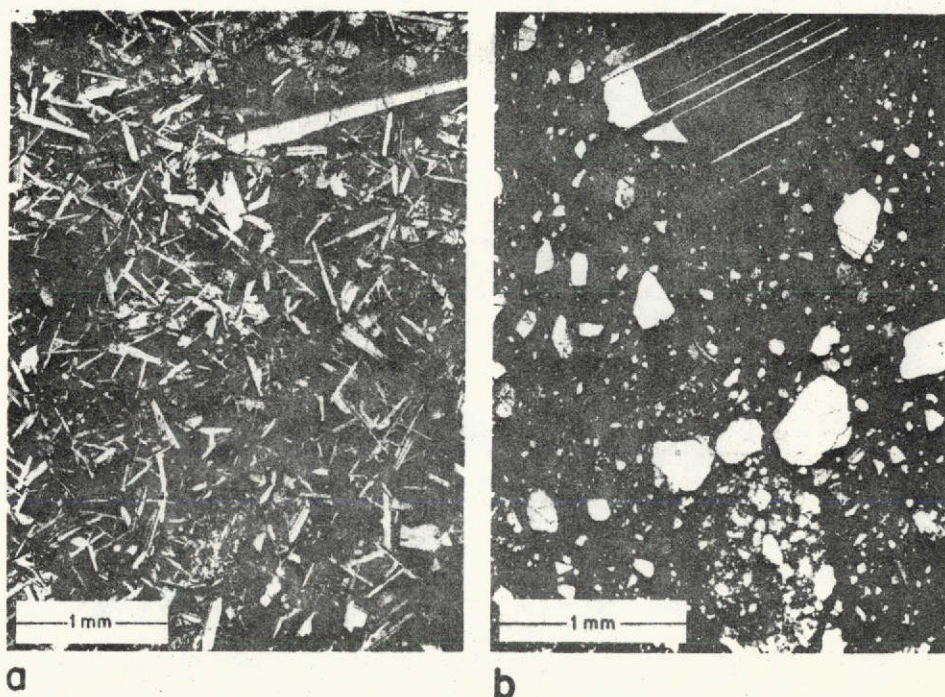
H. -R. WENK, M. ULBRICH, and W. F. MÜLLER

Fig. 1. (a) Photomicrograph of subophitic basalt 14310. Crossed nicols. Notice the range in grain size of plagioclase, and the areas with extremely fine-grained anorthite needles. (b) Photomicrograph of breccia 14319. Crossed nicols. Notice a large anorthite crystal and a breccia fragment.

and opaque minerals. The texture is subophitic. Plagioclase ranges greatly in size. The largest crystals in the thin section are 2 mm long, but most of them range between 0.3 and 0.5 mm. Chemical analysis indicates that there are two groups of plagioclase present; these, however, are not apparent by grain size, shape, or texture. An average of microprobe analyses on many crystals gives a composition An 86.9, Or 1.44 for one group and An 94.0, Or 0.42 for the other. Of special interest is the large difference in potassium. These two groups are quite distinct, without intermediate compositions. No zoning has been found except for one very large crystal, which shows a thin rim of the potassium-rich phase; therefore, this An-poor and Or-rich plagioclase may be younger than the other crystals. There are small areas of very fine-grained plagioclase needles chemically indistinguishable from the Or-poor, large ones that show polysynthetic twinning. These "clots" have almost no interstitial pyroxene. Twin laws identified on the U-stage are albite, Carlsbad, albite-Carlsbad (common), pericline (less common), Baveno-r (one crystal only). Cruciform intergrowth is quite common. Attention has been given to the commonly occuring pseudotwins and peculiar intergrowths.

In one group of crystals, the plane between two intergrown crystals looks like a "composition plane" of a twin (Fig. 2a). The two indicatrices are related by a single

rotation as in a regular twin, but neither axis nor composition plane is a rational direction. The composition plane is in the vicinity but distinctly different from (021) (Fig. 2b). These "irrational" intergrowths are not uncommon in lunar and meteoritic plagioclase (Ulbrich, 1971; Wenk and Nord, 1971).

In another case (Fig. 2c), three crystals are intergrown. Crystal 1–2 is a regular albite-Carlsbad twin with (010) as composition plane; 2–3 is a pericline twin, whose composition plane should be the rhombic section which is close to (001) for anorthite. The actual plane of intergrowth in these crystals is a rough surface close to (010) (Fig. 2d).

Pyroxenes have not been studied in detail. Routine checks showed that clino-pyroxenes with small $2V_\gamma$ (12–22°) twinned on (100) are common. No exsolution lamellae were seen in the petrographic microscope. Orthopyroxene (hypersthene) is less common and frequently mantled by pigeonite. A similar type of intergrowth as described for plagioclase (Figs. 2c, d) has been found in pyroxene. Fig. 2e is an example of polysynthetically twinned pigeonite (1–2) ([010] common axis = Y), yet the composition plane 1–2 is not (100) but an irrational and slightly curved surface (C.P. 1–2, Fig. 2f). This twinned crystal is partly rimmed by another clino-pyroxene (3), which appears to be more iron-rich, because it has the same optical orientation as 2 ($X_2 = X_3$, $Y_2 = Y_3$, and $Z_2 = Z_3$), but has a higher birefringence and higher $2V_\gamma$.

A fragment from 14162 coarse fines has properties very similar to that of 14310 basalt. Textures are identical and two groups of plagioclase are present. We assume that it is a fragment of the same rock.

A large number of plagioclase fragments appear in 14319 breccia (Fig. 1b). Plagioclase is heterogeneous: many crystals are twinned, some are undeformed, some are fractured, some have patchy extinction and bent lamellae. One crystal of plagioclase shows very thin platelets of an opaque mineral on (010). Other components of the breccia are ortho- and clinopyroxene with exsolution and twin lamellae, perovskite, and an unidentified small fragment of a yellow biaxial positive crystal. Apart from crystal fragments, the breccia contains many lithic fragments. Euler angles of plagioclase have been determined in anorthositic and gabbroic fragments. A basalt fragment appears to be closely related to basalt 14310. In the breccia there also are fragments of an older breccia. Brown glass inclusions show beginning crystallization. Noteworthy are spherical aggregates of pyroxene with radial crystallites, resembling meteoritic chondrules. Many lithic and crystallite fragments in the breccia are rounded; others, however, have sharp corners.

Sample 12021 is a basalt of ophitic texture. Some of the large plagioclase crystals are skeletal with pyroxene and opaque inclusions.

Calcic plagioclase from terrestrial rocks and from eucrite meteorites with similar mineralogical composition has been analyzed and compared with the lunar crystals. Some results on meteoritic plagioclase are included here, because, to our knowledge, this paper gives the first description of optical properties of plagioclase in such meteorites. The eucrites are composed of calcic plagioclase, and pigeonite with exsolution lamellae of subcalcic augite to augite. Cachari (Argentina) is brecciated, Serra de Magé (Brazil) shows a beautiful equigranular texture, Ibitira (Brazil) has
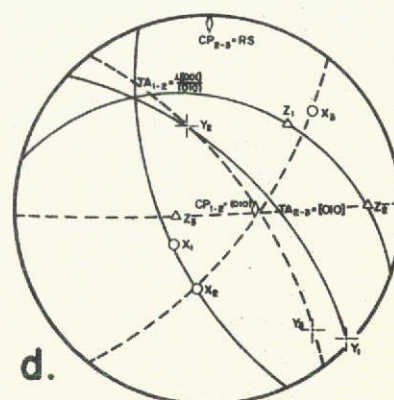
anorthite

a.

b.

—— 1-2 Albite – Carlsbad
––– 1-3 irrational
······ 2-3 irrational

anorthite
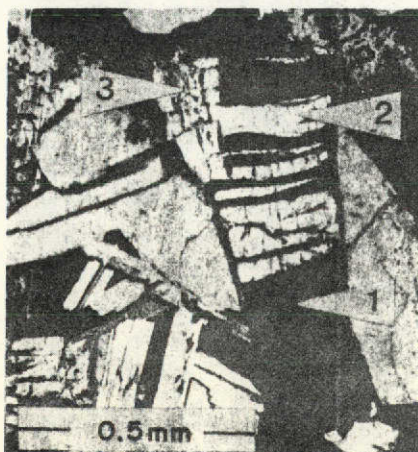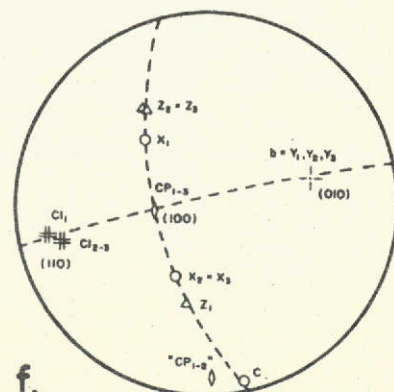

c.

d.
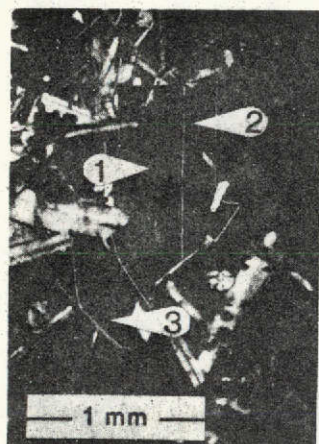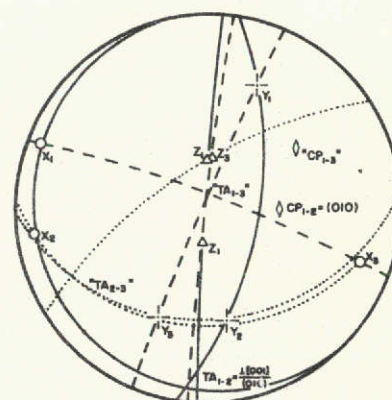
—— 1-2 Albite – Carlsbad
––– 2-3 Pericline

Pigeonite

e.

f.

few large crystals and a ground mass of fine annealed grains with polygonal outlines. Plagioclase in all of them is twinned after the albite, albite-Carlsbad, Carlsbad, and pericline laws (Ulbrich, 1971).

U-STAGE ANALYSIS OF PLAGIOCLASE

Euler angles are used to describe the orientation of the optical indicatrix in the crystal. Euler I angles (Θ, Ψ, and Φ) have been derived from measurements of the albite composition plane (010) and the albite-Carlsbad twin axis $\perp$[001] in (010), and in some cases, from the cleavage (001). The results are listed in Table 1. In order to evaluate the use of the orientation of the indicatrix as an indicator for the thermal history, we plot the angles Φ and Ψ, which show the largest variation in calcic plagioclase, as a function of the anorthite content (Fig. 3). For reference we also plot all data on calcic plagioclase found in the literature and add new measurements. This gives a better measure of the significance of an interpretation than if we compare the new data points with averaged determinative curves (Burri et al., 1967). Above An 75 there are no longer two distinct curves for plutonic and volcanic plagioclase; there is, instead, a diffuse band of scattering points. To make any statement about the thermal history of the rock, a statistical number of high-precision measurements is necessary. It is difficult also to predict the chemical composition in this range of the plagioclase series with accuracy greater than ± 5 to 10% An. The scatter in the data is larger than the accuracy of the measurements and we expect that in addition to the chemical composition and the thermal history, submicroscopic features such as twins and domains may account for it. Looking at all anorthites, Φ and Ψ appear to be slightly larger for plutonic than for volcanic feldspars, and the rather large angles in lunar and meteoritic plagioclase agree with plutonic optics (Wenk and Nord, 1971; Ulbrich, 1971; E. Wenk et al., 1972). As has been shown by E. Wenk et al. (1972), in $\Phi\Psi$ plots our data scatter in the same field as theirs. The $\Phi\Psi$ plots also indicate that lunar plagioclase may have slightly different optical properties than terrestrial ones. To prove this, very pure anorthites have to be studied.

Fig. 2. Unusual twins in lunar basalt 14310. Photomicrographs and stereographic projection in upper hemisphere are in the same orientation. (a), (b): anorthite showing irrational intergrowth between crystals 1 and 3. The pseudocomposition plane, CP 1–3, is close to but different from (021). The "twin axis" 1–3 is also irrational. Crystals 1 and 2 are in albite-Carlsbad relation. (c), (d): anorthite with albite-Carlsbad (1–2) and pericline twin (2–3). The 2–3 composition plane (rhombic section) should be close to (001). The actual plane of intergrowth is close to (010). (e), (f): Polysynthetically twinned pigeonite (1–2). The common axis between 1 and 2 is [010] = Y. The plane of intergrowth (C.P. 1–2) is not the theoretical composition plane (100), but an irrational surface. The twinned crystal is rimmed by another clinopyroxene, which is in the same optical orientation as 2 but has higher 2V$_y$ (3).

Table 1. Euler I angles and chemical composition of plagioclase from lunar rocks and eucrite meteorites. The accuracy of Euler angles is $\pm 1/2°$.

Lunar Rocks	Twin laws	$2V_a$	Φ	Ψ	Θ	An	Or	Ab
12021, 118C basalt fragment	Ab, Ca Ab-Ca, Pe	77	$25\frac{1}{4}$	−6	36	92.9	0.34	6.7_4
14310, 23 & 95 plagioclase-pyroxene basalt	Ab, Ca, Ab-Ca	—	$25\frac{1}{2}$	−2	38	85.3_0	1.72	12.9_8
	Pe (rare) Baveno-r	—	25	−4	38	87.6_9	1.22	11.0_9
	(only one)	81	$23\frac{3}{4}$	$-5\frac{1}{2}$	38	87.6_0	1.38	11.0_2
		77	22	$-5\frac{1}{2}$	37	93.0_0	0.48	6.4_3
		78	24	−6	34	94.3_3	0.39	5.2_8
		—	$23\frac{1}{2}$	−6	38	93.4_1	0.45	6.1_4
14319, 6 Breccia	Ab, Ca							
(A) plag.-pyr. aggr. (anor.)	Ab-Ca Pe	79 78	$22\frac{3}{4}$ $21\frac{1}{2}$	−4 −7	38 37	93.8_9 94.6_1	0.37 0.54	5.7_4 4.8_5
(B) plag.-pyr. aggr. (gab.)	Ab, Ca Ab-Ca, Pe	—	20	−6	37	92.6_9	0.63	6.6_8
(C) plag. aggregate	Ab, Ca Ab-Ca	—	26	−1	34	84.2_3	1.56	14.2_1
(D) plag. frag.	Ab	—	23	−8	41	96.7_0	0.39	2.9_1
14162, 13 coarse fines	Ab, Ca Ab-Ca	—	23	$-6\frac{1}{2}$	38	93.5_6	0.44	6.0_0
plag.-pyrox. in the fines	Pe (rare)	—	17	−10	$37\frac{1}{2}$	93.7_3	0.31	5.9_6
Eucrite Meteorites								
Serra de Mage	Ab, Pe	—	20	$-8\frac{1}{2}$	$37\frac{1}{2}$	94.8_3	0.09	5.0_8
	Ca, Ab-Ca	77	23	−6	38	95.3_7	0.04	4.5_9
Ibitira	Ab-Ca,	81°	$22\frac{3}{4}$	−6	37	95.3_0	0.21	4.4_9
Cachari	Ab, Ca, Pe	—	28	−6	42	88.2_9	0.45	11.2_5

Ab: Albite; Ca: Carlsbad; Pe: Pericline.

LATTICE CONSTANTS AND STRUCTURE

Lattice constants were measured on x-ray precession photographs, which were used to determine the structural state from the presence and diffuseness of indicative b- and c-reflections. The lattice parameters along with other structural information for four crystals are listed in Table 2. The variations are within the standard deviation and no conclusions can be drawn. Except for crystals from 10017, all analyzed crystals showed a transitional anorthite structure with strong b-reflections and diffuse c-reflections streaking parallel to b^* in 0kl sections. As has been pointed out by Gay (1953), Gay and Taylor (1953), and Laves and Goldsmith (1954a, b), the diffuseness of c-reflections is a function of the chemical composition and of the thermal history. Comparing lunar crystals with terrestrial and eucrite anorthites *of*
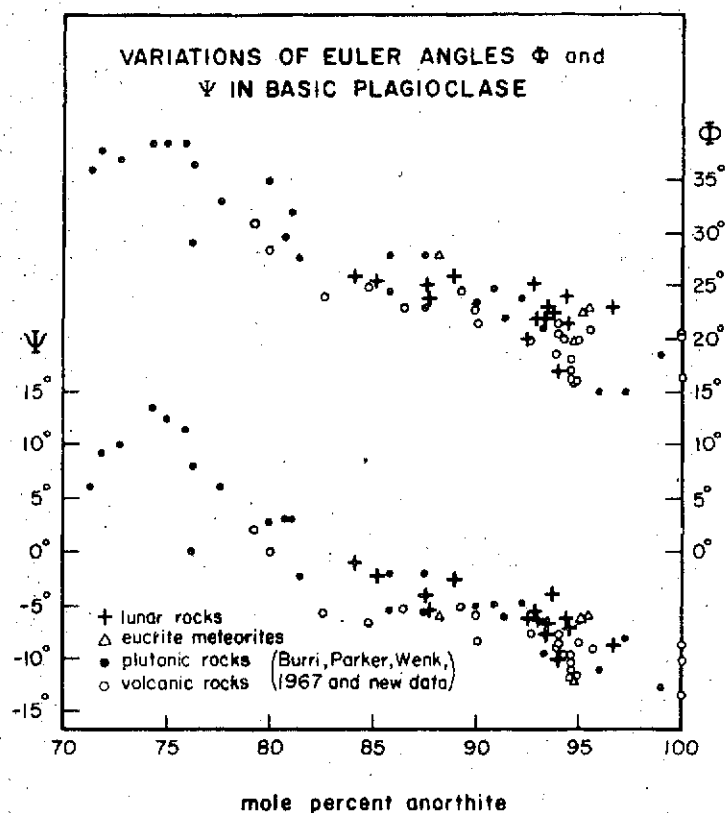
Fig. 3. Variation of Euler angles Φ and Ψ as a function of chemistry in anorthites. Data from the literature and new measurements.

Table 2. X-ray data of anorthites from precession photographs.

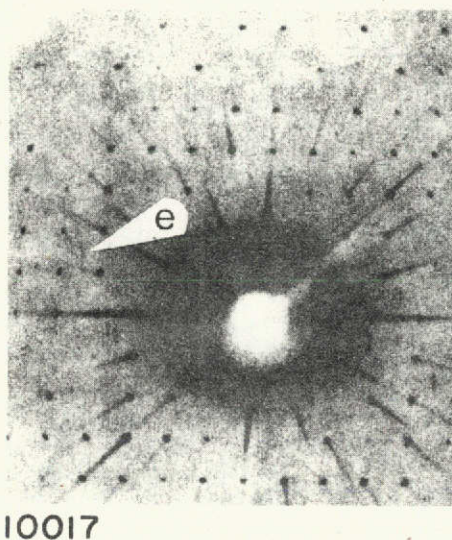| Sample	a	b (A)[1]	c	α	β (degrees)[2]	γ	Structure	An	Or	Ab
10017 (A)	8.19	12.87	14.18	93.1	116.1	90.9	b weak			
10017 (B)							e (b-split) and b			
12021 (A)	8.18	12.87	14.18	93.3	115.9	90.9	b sharp, strong c diffuse, streaks along b^*	92.0₆	0.42	7.5₂
12021 (B)							b sharp, strong c diffuse, streaks along b^*			
12021 (C)							b sharp, strong c diffuse, streaks along b^*			
14310	8.18	12.87	14.19	93.3	116.2	91.0	b sharp, strong c diffuse, streaks along b^*	93.4₄	0.16	6.4₀
Serra de Magé eucrite	8.19	12.9	14.18	92.9	116.1	91.4	b sharp, weak c sharp, strong	95.5₇	0.05	4.3₉

[1]error ± 0.01 Å   [2]error ± 0.1°

IOOI7

Fig. 4. X-ray single-crystal precession photograph (0kl). (Mo-radiation, Zr filter) of a plagioclase crystal in rock 10017. Notice asymmetric e-reflections and sharp b-reflections in the same crystal.

the same chemical composition, the structure of lunar plagioclase is similar to that of plagioclase from volcanic rocks. All comparative metamorphic, plutonic and meteoritic feldspars that have been studied by the authors show much stronger and sharper c-reflections (Wenk and Nord, 1971; Müller *et al.*, 1972). Of special interest is a crystal from 10017 that shows $e(b$-split)-reflections and sharp b-reflections in the same crystal (Fig. 4). Similar patterns have been observed by Jagodzinski and Korekawa (1972) in terrestrial An 70–77 plagioclase and have been interpreted as exsolution of an An 65 and an An 80 end member. We did not find that lunar plagioclase is "intimately twinned" on a submicroscopic scale according to the albite-Carlsbad law (Czank *et al.*, 1972). The x-ray patterns of 14310 plagioclase and other crystals analyzed indicate perfect single crystals.

ELECTRON MICROSCOPY

High voltage (650 kV) transmission electron microscopy of plagioclase was done on specimens from 14310. Isolated submicroscopic twin lamellae were observed (Fig. 5a). They commonly occur singly or as two to three parallel lamellae, approximately 1 micron wide, with a few lamellae as small as 0.2 microns. Twin laws identified were albite and Baveno-r. It is not known what influence these submicroscopic twins have on the U-stage determined orientation of the indicatrix. Possibly they account for the difficulty in obtaining perfect extinction in the optical measurements. Selected-area electron diffraction patterns showed sharp a- and b-, diffuse c-, and very weak, diffuse d-reflections. The c- and d-reflections were streaked in
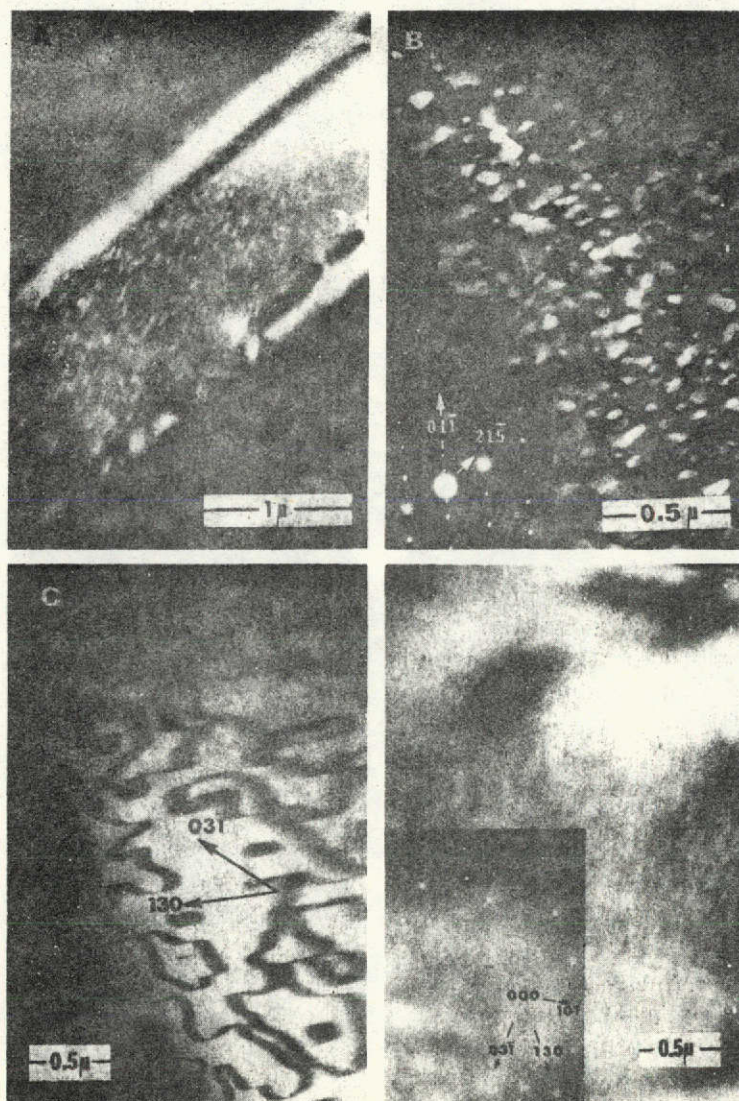
Fig. 5. High voltage (650 kV) transmission electron micrographs of plagioclase from 14310. (a) Baveno-r twin lamellae with *b*-antiphase-domain boundaries in contrast. Dark-field image with $\vec{g} = 011$ as the operating beam. (b) Small *b*-antiphase domains. Dark-field image with $\vec{g} = 31\bar{5}$. The selected area electron diffraction pattern is inserted. (c) Boundaries of *b*-antiphase domains. Dark-field image with $\vec{g} = 03\bar{1}$. Note the larger domain size compared to (b). (d) Cross-hatched structures. Dark-field image with $\vec{g} = 130$. The corresponding selected area diffraction pattern (insert) displays "*b*-split" reflections. Different part of the same crystal as in (c). Note radiation tracks.

directions perpendicular to about (231) in a diffractogram normal to [211]. This agrees with x-ray studies by Ribbe and Colville (1968) and electron diffraction results by Appleman et al. (1971). Dark-field images using b-reflections revealed smoothly curved antiphase-domain boundaries (Figs. 5a, b and c). Most of these b-antiphase domains were 500–1000 Å wide (Fig. 5b) but in some cases larger b-domains have been observed in the same specimen (3000–10,000 Å, Fig. 5c; compare also Christie et al., 1971). No c-domains could be resolved in dark-field images exposed for as much as two minutes. Of special interest was a crystal with a range of chemical composition, probably similar to the one described in the section on petrography, which had a composition of An 94 in the core and had a rim of An 87 bytownite. This crystal shows in one part very large b-domains (Fig. 5c). No c-domains could be imaged. The crystal is bordered by a 2.5 micron broad band of a plagioclase phase that displays strong b-split reflections and very small b-domains in dark-field pictures. In this crystal a cross-hatched structure resembling peristerite was seen (Fig. 5d). The same structure has been observed by Lally et al. (1972) and may represent an exsolution in the bytownite composition range (Nissen, 1968; Jagodzinski and Korekawa, 1972). Radiation tracks can be seen in the same picture (Fig. 5d) with a maximum track density of about 2×10^8 cm^{-2}. The presence of b-domains and the absence of c-domains has been seen in at least 15 of the crystals that were examined. This makes it very probable that many of these anorthites have the far more common An 94–95 composition. The diffraction patterns agree with the x-ray precession photographs of the crystal that had a chemical composition of An 93.4.

Müller et al. (1972) found that anorthites (An 95–97) from a metamorphic calc-silicate rock and a eucrite meteorite contained c-antiphase-domain boundaries, the domain walls being as much as a few microns apart, whereas an anorthite (An 95) from a volcanic tuff displayed only small c-domains of the order of 70 to 100 Å in diameter. In view of these observations, it appears that the fact that no c-domains could be imaged in anorthite from rock 14310, which showed more diffuse c-reflections than all comparative terrestrial anorthites of similar chemical composition, can be interpreted as an indication for relatively rapid cooling of 14310. This characterization is not in disagreement with the results of other investigators who describe 14310 as having been more slowly cooled than other lunar basalts (e.g. Finger et al., 1972). The distinction suggested by structural variations of anorthite so far is merely between a volcanic and a plutonic/metamorphic geological history. Other lunar igneous rocks may have had a different history than 14310. Large c-antiphase domains were observed in the anorthite of 15415 anorthosite (Lally et al., 1972), which indicates that this rock may have formed under plutonic conditions.

REFERENCES

Appleman D. E. Nissen H. -U. Stewart D. B. Clark J. R. Dowty E. and Heubner J. S. (1971) Studies of lunar plagioclases, tridymite, and cristobalite. *Proc. Second Lunar Sci. Conf., Geochim. Cosmochim. Acta* Suppl. 2, Vol. 1, pp. 927–930. MIT Press.

Burri C. Parker R. L. and Wenk E. (1967) *Die optische Orientierung der Plagioklase.* Birkhäuser, Basel.

Christie J. M. Lally J. S. Heuer A. H. Fisher R. M. Griggs D. T. and Radcliffe S. V. (1971) Comparative electron petrography of Apollo 11, Apollo 12 and terrestrial rocks. *Proc. Second Lunar Sci. Conf., Geochim. Cosmochim. Acta* Suppl. 2, Vol. 1, pp. 69–89. MIT Press.

Czank M. Girgis K. Harnik A. B. Laves F. Schmid R. Schulz H. and Weber L. (1972) Crystallographic studies of some Apollo 14 plagioclases (abstract). In *Lunar Science—III* (editor C. Watkins), pp. 171–173, Lunar Science Institute Contr. No. 88.

Finger L. W. Hafner S. S. Schurmann K. Virgo D. and Warburton D. (1972) Distinct cooling histories and reheating of Apollo 14 rocks (abstract). In *Lunar Science—III* (editor C. Watkins), pp. 259–261, Lunar Science Institute Contr. No. 88.

Gay P. (1953) The structures of the plagioclase feldspars: III. An x-ray study of anorthites and bytownites. *Mineral. Mag.* **30**, 169–177.

Gay P. and Taylor W. H. (1953) The structures of the plagioclase feldspars. IV. Variations in the anorthite structure. *Acta Cryst.* **6**, 647–650.

Jagodzinski H. and Korekawa M. (1972) X-ray studies of plagioclases and pyroxenes (abstract). In *Lunar Science—III* (editor C. Watkins), pp. 427–429, Lunar Science Institute Contr. No. 88.

Lally J. S. Fisher R. H. Christie J. M. Griggs D. T. Heuer A. H. Nord G. L. Jr. and Radcliffe S. V. (1972) Electron petrography of Apollo 14 and 15 samples (abstract). In *Lunar Science—III* (editor C. Watkins), pp. 469–471, Lunar Science Institute Contr. No. 88.

Laves F. and Goldsmith J. R. (1954a) Long-range short-range order in calcic plagioclases as a continuous and reversible function of temperature. *Acta Cryst.* **7**, 465–472.

Laves F. and Goldsmith J. R. (1954b) On the use of calcic plagioclases in geologic thermometry. *J. Geol.* **62**, 405–408.

Müller W. F. Wenk H. -R. and Thomas G. (1972) Structural variations in anorthite. *Contr. Mineral. Petrol.* **34**, 304–314.

Nissen H. U. (1968) A study of bytownites in amphibolites of the Ivrea Zone (Italian Alps) and in anorthosites: A new unmixing gap in the low plagioclases. *Schweiz. Mineral. Petrogr. Mitt.* **48**, 53–55.

Ribbe P. H. and Colville A. A. (1968) Orientation of the boundaries of out-of-step domains in anorthite. *Mineral. Mag.* **36**, 814–819.

Ulbrich M. (1971) Systematics of eucrites and howardite meteorites and a petrographic study of representative individual eucrites. M.A. thesis, Univ. of Calif., Berkeley.

Wenk E. Glauser A. Schwander H. and Trommsdorff V. (1972) Optical orientation, composition and twin laws of plagioclase from rocks 12051, 14053 and 14310 (abstract). In *Lunar Science—III* (editor C. Watkins), pp. 794–796, Lunar Science Institute Contr. No. 88.

Wenk H. -R. and Nord G. L. (1971) Lunar bytownite from sample 12032, 44. *Proc. Second Lunar Sci. Conf., Geochim. Cosmochim. Acta* Suppl. 2, Vol. 1, pp. 135–140. MIT Press.

Structural Variations in Anorthites

W. F. Müller
Department of Materials Science and Engineering

H. R. Wenk
Department of Geology and Geophysics

G. Thomas
Department of Materials Science and Engineering
University of California at Berkeley

Abstract. Variations of structure and optical properties in anorthites (An 93–97%) of different origin are analyzed with the petrographic microscope, U-stage methods, X-ray single crystal analysis and high voltage electron microscopy. No significant variation has been found in the orientation of the indicatrix and of the lattice constants. But c-type reflections ($h + k$ even, l odd) are strong and sharp in anorthites from slowly cooled rocks and diffuse in anorthites of identical chemical composition from quenched igneous rocks. Large type c-antiphase domains (5000–10000 Å) are found in the slowly cooled rocks, c-domains in volcanic rocks are small (100 Å) or could not be imaged. The presence of only b-domains in lunar basalt 14310 indicates quenching of this rock. Large c-domains in the Apollo 15 genesis rock (15415, Lally *et al.*, 1972) indicate slow cooling similar to terrestrial metamorphic rocks.

Introduction

Of all feldspars calcic plagioclase has been least studied and many of its structural properties are still unclear. Smith and Ribbe (1969) give a summary of the present knowledge on the plagioclase structures and for all details we refer to that paper. In pure anorthite the Al—Si distribution in the tetrahedral framework is essentially ordered (Kempster *et al.*, 1962; Megaw *et al.*, 1962; Wainwright and Starkey, 1971) in agreement with the aluminum-avoidance principle (Loewenstein, 1954). This order persists up to high temperatures (Laves and Goldsmith, 1955). The ordering of Al—Si causes a doubling of the c-axis which is expressed in the appearance of additional reflections in the diffraction pattern.

There are four classes of reflections (Fig. 2). Type-a-reflections ($h + k$ even, l even) are due to the basic feldspar structure. They are the only reflections present in alkali-feldspars. Type-b-reflections ($h + k$ odd, l odd) are attributed to Si-Al order. They are present in anorthite and become increasingly diffuse with lower An-content and disappear around An 70%. Bytownites show only these a- and b-reflections. The corresponding structure is named *body-centered anorthite*. Type-c-reflections ($h + k$ even, l odd) and d-reflections ($h + k$ odd, l even) occur in anorthite only. They are sharp in slowly cooled crystals with An 95% (*primitive anorthite*) and diffuse with streaking in quenched and Na-rich anorthite (*transitional anorthite*). Upon heating the c-reflections of primitive anorthite become more diffuse and disappear below 350° C. These changes occur immediately and

are reversible (Brown et al., 1963; Bruno and Gazzoni, 1967; Foit and Peacor, 1967; Laves, Czank and Schulz, 1970). Therefore they are interpreted as caused by a displacive phase change and not a diffusive transformation (Laves and Goldsmith, 1961; Megaw, 1962). The structure determination of primitive anorthite (Kempster et al., 1962; Wainbright and Starkey, 1971) in fact suggests that there are two statistically overlapping Ca-positions or that there is strong anisotropic thermal vibration of the Ca-atom in the tetrahedral framework which produces the primitive $c = 14$ Å unit cell. At lower anorthite content order/disorder of Si/Al causes distortions of the lattice and small amounts of disorder may be important in the nucleation of primitive anorthite domains (Smith and Ribbe, 1969). The Si-content i.e. the framework constitution and not so much the Ca/Na ratio appears to have the most important influence on the structure in sodium bearing anorthite. The purpose of this study was to investigate structural variations in anorthites of different origin. Crystals of similar chemical composition and different thermal history are characterized by their optical properties, their crystal structure and their microstructure. Since the pioneering work of McConnell and Fleet (1963), Nissen and Bollmann (1966), Ribbe (1962), electron microscopy has become a very powerful tool in the study of feldspars. We applied this method to anorthites with the special aim to make transmission electron microscopy more popular in mineralogy and petrology. The present contribution is only concerned with *natural crystals*. In a second stage we will try to reproduce the observed structures in the laboratory.

Petrography

The only thing which the four specimens chosen for this analysis have in common is that they all contain plagioclase with an anorthite content ranging from 93 to 97%. Locations, textures, origin, age and mineralogical composition are about as different as can be (Fig. 2).

The first specimen coming from the Fra Mauro area on the moon (Apollo 14, specimen 14310) is an ilmenite bearing, anorthite rich ortho-clinopyroxene basalt of subophite texture (Fig. 2a, cf. Wenk et al., 1972).

Another volcanic rock is an anorthite-pigeonite tuff, very rich in euhedral anorthite crystals and two glass phases from Miyake Island, Tokyo Bay, Honshu, Japan (Fig. 2b 16707 cf. Leisen, 1934; Kôzu, 1914).

302 is a eucrite meteorite from Serra de Magè, Brasil (Ulbrich, 1971). The mineralogical composition is granular anorthite and pigeonite with "myrmekitic" exsolutions of augite (Fig. 2c).

Sci 59 is metamorphic calcsilicate rock of miocene age from V. Schiesone (Bergell Alps, N. Italy, cf. Wenk, 1970). The slightly foliated specimen consisting of diopside, hornblende, anorthite, calcite, sphene and ore bearing shows typical annealing textures (Fig. 2d) and is one of the slowly cooled amphibolite facies rocks of the Lepontine zone (E. Wenk, 1962).

The *optical properties* of plagioclase, especially the orientation and shape of the indicatrix in the triclinic crystal, vary greatly with the chemical composition and thermal history. Euler I angles are used to describe the orientation of the indicatrix. For sodium rich plagioclase the data for volcanic and plutonic plagioclase

Table 1. Euler 1 angles relating the optical indicatrix and crystal coordinates. Accuracy of Euler angles is $\pm^1/_2°$

Specimen	Twin-laws	$2V\alpha$	Θ	Ψ	Φ	An	Or	Ab
			in degrees			in mole percent		
14310 lunar	Ab, Ca,		$25^1/_2$	-2	38	85.3_0	1.72	12.9_8
plag. pyrox.	Ab-Ca		25	-4	38	87.6_9	1.22	11.0_9
basalt	Pe (rare)	81	$23^3/_4$	$-5^1/_2$	38	87.6_0	1.38	11.0_2
	Baveno	77	22	$-5^1/_2$	37	93.0_9	0.48	6.4_3
	right	78	24	-6	34	94.3_3	0.39	5.2_8
			$23^1/_2$	-6	38	93.4_1	0.45	6.1_4
Volcanic	Ab, Ca		$20^1/_4$	-10	34	94.3_0	0.06	5.1_0
tuff,	Ab-Ca		21	-9	34	95.6_4	0.07	4.2_9
Miyake			16	$-11^1/_2$	34	94.5_2	0.01	5.4_7
Is. Japan			20	$-8^1/_2$	$36^1/_2$	94.9_9	0.09	4.9_2
			$20^1/_2$	-8	37	93.9_9	0.06	5.9_5
			23	-6	35	—	—	—
Serra de Mage	Ab, Ca,		20	$-8^1/_2$	$37^1/_2$	94.8_3	0.09	5.0_8
eucrite	Ab-Ca	77	23	-6	38	95.3_7	0.04	4.5_9
meteorite	Pe							
Sci 59 diops.	An, Pe,	77	15	-8	37	97.4	0.01	2.5_9
calc. anorth.	Ab-Ca							
hbl. fels.	(rare)							
V. Schiesone,								
(Alps)								

Ab   albite,
Ca   Carlsbad,
Ab-Ca albite-Carlsbad,
Pe   pericline.

follow two distinctly different curves (Burri, Parker, Wenk, 1968). These curves join at An 90% and from there on to pure anorthite a broad band of irregularly scattering points characterizes the orientation (Fig. 1). The band for ψ and ϕ is about 18 degrees wide which is well beyond statistical scatter due to errors in the measurements. Euler I angles for the four specimens studies in this paper are listed in Table 1. There is no significant difference between the two quenched volcanic anorthites and the slowly cooled meteoritic and metamorphic crystals. Thus the orientation of the indicatrix, which is a convenient parameter to describe sodium rich plagioclase, looses its diagnostic value in the anorthite range and other parameters have to be found. Such a parameter as has been mentioned in the introduction is the *crystalstructure* expressed in the absence, presence or diffuseness of b and diffuse c-reflections. X-ray precession photographs (Fig. 2) show for the volcanic samples (Fig. 2 e, g) a transitional anorthite pattern with sharp b and c reflections which are streaking approximately parallel to b^* in 0kl photographs and for the slowly cooled samples (Fig. 2g, h) they show a primitive anorthite structure with strong and sharp c-reflections. There is a clear variation in diffuseness of c-reflections of chemically identical anorthites and comparison

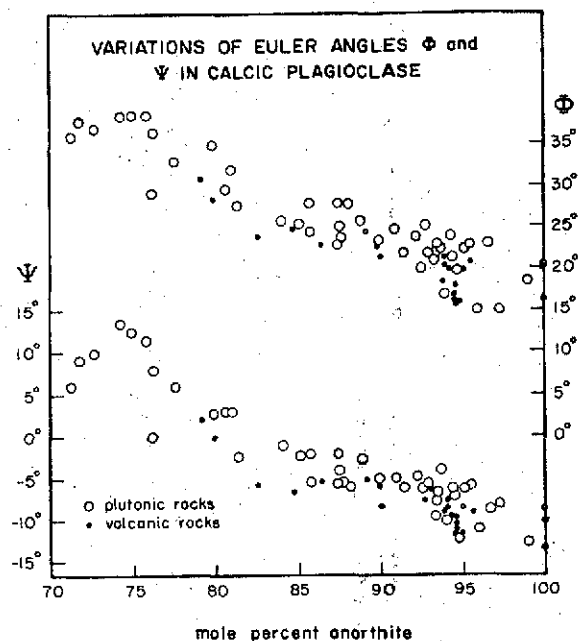VARIATIONS OF EULER ANGLES Φ and Ψ IN CALCIC PLAGIOCLASE

Fig. 1. Variation of Euler angles Φ and Ψ which characterize the orientation of the optical indicatrix in the crystal for calcic anorthites (data are from the literature)

mole percent anorthite

Table 2. Lattice constants and structure of anorthites (from precession photographs)

Specimen	a_0	b_0	c_0	α	β	γ	Structure	An	Or	Ab
	Å error is ± 0.01 Å			in degrees, error is $\pm 0.1°$				in mole percent		
14310 lunar plag. pyrox. basalt	8.18	12.87	14.19	93.3	116.2	91.0	transitional	93.4_4	0.16	6.4_0
Volcanic tuff Miyake Isl. Japan	8.17	12.87	14.17	93.2	115.8	91.2	transitional	95.4_7	0.02	4.5_4
Serra de Magè Eucrite Meteorite	8.19	12.88	14.18	92.9	116.1	91.4	primitive	95.5_7	0.05	4.3_9
Sci 59 diops. hbl. calc. anorth. fels. V. Schiesone, (Alps.)	8.18	12.89	14.19	93.3	116.0	91.1	primitive	97.1_6	0.25	2.5_9

of the lunar 14310 crystal with the anorthite in the Japanese volcanic tuff indicates that the crystalstructure of both crystals is very similar. Lattice parameters, taken from precession photographs do not show a significant variation (Table 2).

Photomicrograph X-Pol.   X-Ray Precession

Lunar basalt,
14310

Volcanic tuff,
Japan

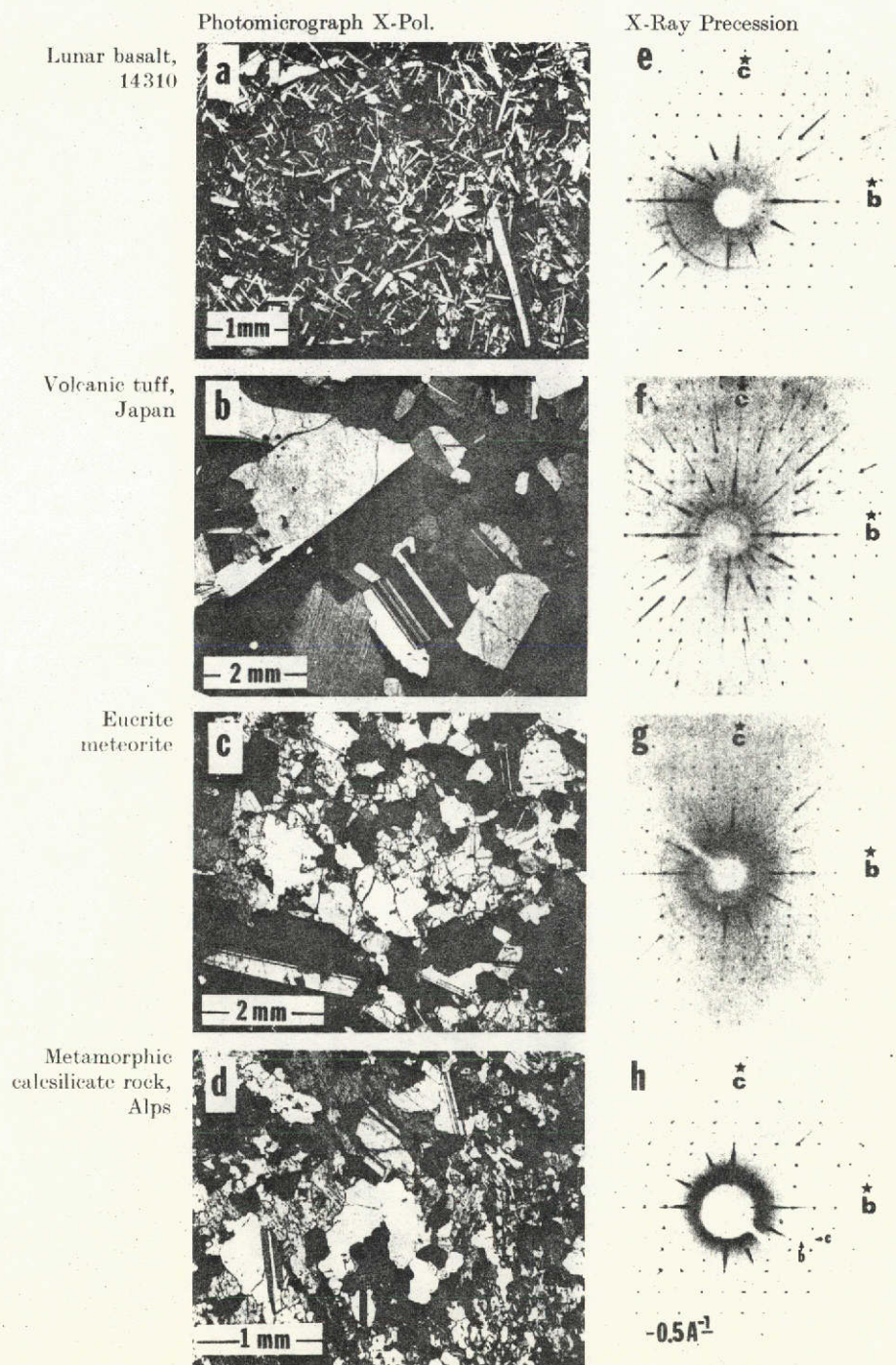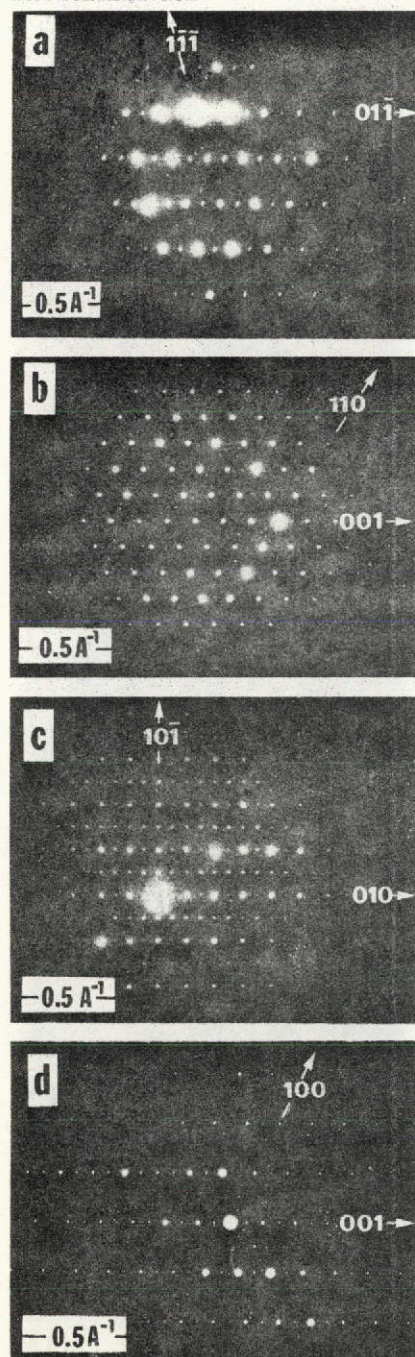Eucrite
meteorite

Metamorphic
calcsilicate rock,
Alps

Fig. 2. a–d Photomicrographs using a petrographic microscope with crossed nicols. e–h X-ray single-crystal precession-a photographs (*Mo* radiation, *Zr* filter)

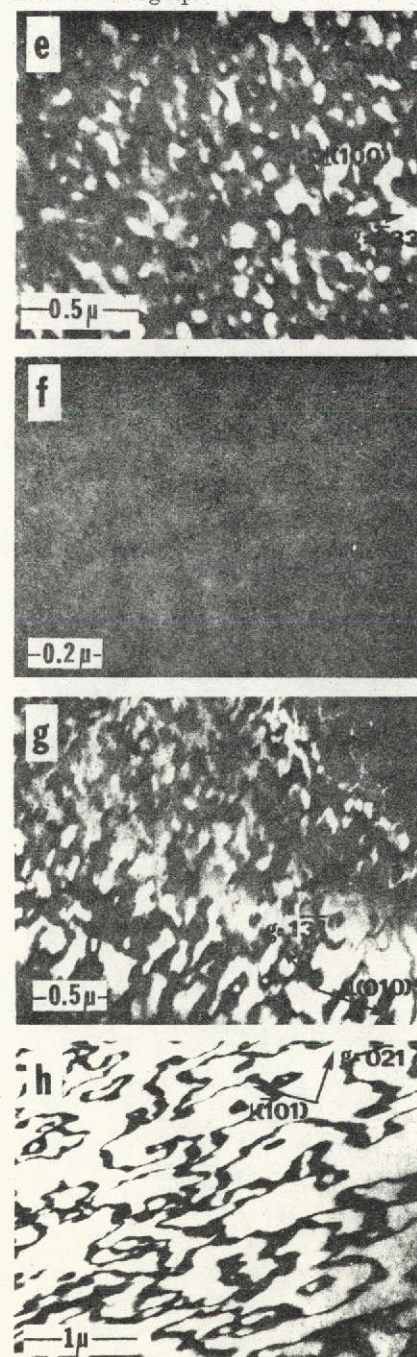Electrondiffraction   Electronmicrograph

Fig. 3a–d. Selected area electron diffractograms. a–c 650 kV, d 500 kV acceleration voltage. e–h Transmission electron micrographs. e Type b, f–h type c-domains. Dark field. The operating diffracted beam $\bar{g}$ is indicated. 650 kV acceleration voltage.
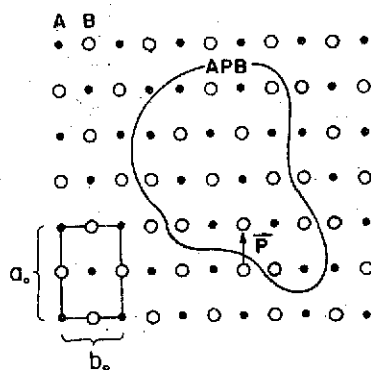
Fig. 4. Schematic representation of an antiphase domain boundary (APB) in an hypothetical alloy with atoms A (dots) and B (circles). p is called the displacement vector or antiphase vector. a_0 and b_0 are the lattice constants

Transmission Electron Microscopy

A Hitachi HU650 electron microscope with 650 kV acceleration voltage was used for the electron microscopic studies. Thinned specimens suitable for electron transmission were obtained from standard petrographic thin sections by ion-bombardment (Castaing, 1955; for experimental details see Barber, 1970; and Radcliffe et al., 1970). Due to the increased penetrating power of the high voltage electron microscope compared to a 100 kV electron microscope and to the preparation method large areas could be examined.

It may be useful to discuss briefly some basic principles of order-disorder transformations, antiphase domain boundaries and transmission electron microscopy. For details the reader is referred to review articles by Marcincowski (1963), Cohen (1970) with a discussion by Warlimont (1970), and to textbooks on transmission electron microscopy (Thomas, 1962; Amelinckx, 1964; Hirsch et al., 1965). We consider an alloy with 50% atoms A and 50% atoms B crystallizing in a structure in which the atomic positions are randomly occupied by the atoms A and B. If the alloy cools below a critical temperature, ordering of the atoms may take place. In the ordered structure, called a superstructure of the disordered one, all atoms A have atoms B as their closest neighbors and vice versa (Fig. 4). Ordered domains may nucleate and begin to grow at different places within the same disordered crystal. When these ordered domains impinge on each other they may either fit perfectly together forming a single crystal or they may meet each other "out of phase" or "out of step". In this case a boundary called an *antiphase domain boundary* (APB) is produced between the domains. The region enclosed by an APB is called an *antiphase domain*. The antiphase vector $\bar{p}$ describes the displacement of a particular atom species between two adjacent domains. Thus $\bar{p}$ is the displacement necessary to produce the two domains from a single crystal. Depending on crystal structure there are many possibilities for such vectors. When electrons, characterized by a distinct wavelength λ, encounter a crystalline specimen, part of them will be diffracted on suitable oriented lattice planes under the corresponding Bragg angles $2\Theta_i$. Electron diffraction patterns (3a–d) contain the primary beam and diffracted beams indexed $h_i k_i l_i$ corresponding to the reciprocal lattice vectors $\bar{g}_i$. Image contrast is obtained using an aperture by which a distinct beam can be selected to pass through to the final image. The other

beams are withheld. If only the primary beam is allowed to pass a so-called bright field image results. If a diffracted beam is selected for image formation a dark field image is obtained. In dark field images those parts of the specimen will be in bright contrast when (sufficient) electrons have been scattered into the corresponding Bragg reflection. Therefore, taking a superstructure reflection for imaging the regions of the specimen will appear bright which contain the superstructure. If the crystal obtains APB's they may be resolved under certain conditions. Image contrast from APB's depends on several parameters the most important being the phase change associated with the displacement across the boundary. This phase change is given by the phase angle $\alpha = 2\pi \bar{g} \cdot \bar{p}$. A phase jump in the amplitude occurs if $\alpha \neq 0 \mod 2\pi$. i.e. for $\bar{g} \cdot \bar{p}$ non-integral. If $\bar{g} \cdot \bar{p}$ is integral, i.e. when $\bar{p}$ equals a lattice translation vector, α is zero (no contrast). Thus, in general, superlattice diffraction vectors are necessary to provide contrast. If $\alpha = \pi \mod 2\pi$, symmetrical fringes occur about the center of the fault in dark field whereas when $\alpha = 2\pi/3 \mod 2\pi$ symmetrical fringes occur in bright field. However, other factors affect the fringe symmetry, e.g. when the diffraction vectors differ in magnitude but are parallel across the domain wall symmetry properties disappear due to the "excitation error" $\Delta \bar{g}$. This means that the direction of the $\bar{p}$ vector is not easily determined from fringe symmetry but requires careful tilting experiments in order to investigate the same boundary under different reflecting conditions $\{\bar{g}_i \cdot p_i\}$.

Keeping these principles in mind the anorthite specimens have been analyzed and the following features have been observed:

Anorthite from Lunar Basalt 14310. A typical selected area electron diffraction pattern containing sharp *a-* and *b-*reflections and diffuse *c* reflections is shown in Fig. 3a. Very weak and diffuse *d-*reflections were observed. The *c-*reflections were streaked in directions perpendicular to about (231) in a selected area diffractogram normal to [211]. This is in agreement with observations by Ribbe and Colville (1968), Appleman *et al.* (1971), and Christie *et al.* (1971).

Dark field images using *b-*reflections revealed smoothly curved antiphase domain boundaries (Fig. 3e). The size of these domains (500–1000 Å) is distinctly smaller than of those found by Christie *et al.* (1971) in lunar rock 10029. Christie *et al.* (1971) proposed a displacement vector $\bar{p} = (c/2) [001]$. So far, no contrast experiments and calculations have been done to determine the actual displacement vector among the many possibilities.

Anorthite from Miyake Islands, Japan. Selected area electron diffraction pattern show sharp *a-* and *b-* and slightly diffuse *c-*reflections. Small domains in the order of 70–100 Å could be imaged in dark field using type *c-*reflections (Fig. 3f). The *c-*domains in the Japanese anorthite may be ordered domains in a disordered matrix. The type *c-*reflections are less diffuse than those of the lunar anorthite. So we conclude that the *c-*domains in the lunar anorthite were not resolved because they were smaller and probably less ordered than in this anorthite. The occurrence of such small type *c-*domains in lunar rocks was reported by Appleman *et al.* (1971) and Christie *et al.* (1971). Type *b-*domains were not observed in the anorthite from Japan.

Anorthite from the Eucrite Meteorite Serra de Magè. Selected area diffraction patterns show strong *a-* and *b-* and weaker *c-*reflections. The type *c-*reflections

are sometimes slightly diffuse. APB's were visualized in bright field and dark field images using c-reflections (Fig. 3g). The width of mesh of the network formed by the APB's was varying from about 500 to 5000 Å. The domains frequently appear to be elongated parallel to c^*. During the work at the microscope an oscillation of the domain walls has been observed on the screen. Type b-domains were not observed.

Anorthite from Val Schiesone, Alps. Selected area electron diffraction patterns showed strong a-reflections, weaker b- and c-reflections, very weak d-reflections. All reflections were sharp (Fig. 3d). Bright field and dark field images with c-reflections operating revealed large antiphase domains separated by APB's (Fig. 3h). The areas surrounded by APB's as measured in the electron micrographs had a diameter up to several microns. The APB's have apparently a preferential orientation parallel to c^*. Ribbe and Colville (1968) assume an antiphase vector $\bar{p} = {}^1/_2 [\bar{a} + \bar{b} - \bar{c}]$ for the c-domains. For this $\bar{p}$ the phase shift α equals π mod 2π if the diffracted beam $\bar{g}$ is a c-reflection. We observed symmetrical fringe contrast about the center of the APB-fault in dark field. This result would be consistent with the case for the condition $\alpha = \pi$, e.g. it would be consistent with a displacement vector $p = {}^1/_2 [\bar{a} + \bar{b} - \bar{c}]$. But, as noted before for the b-domains, there are also other possibilities which have to be examined by contrast experiments and calculations.

Conclusions

Presence and size of b- and c-antiphase domains in anorthite is a sensitive parameter to characterize calcic plagioclase. The variations in size are influenced by the chemical composition and the thermal and mechanical history. If the An content is known then it is possible to derive the cooling history as is demonstrated by the comparison of the four samples. The size of the domains is a function of nucleation and growth rate. During quenching the domains cannot grow and a pattern of very fine c-domains results which may be partially disordered, causing the diffuse c-reflections. During annealing slightly below the disordering temperature the domains grow. In slowly cooled anorthites (An > 95%) no b-domains were present. It is uncertain if the intensity of c-reflections and shape and size of c-domains is only due to the Ca-position or if Si/Al disorder produced at very high temperatures in the lava has a secondary influence. The c-domains (probably caused by a displacive transformation around 300° C) may reflect only the very late cooling history whereas b-domains (an indication for Al/Si disorder) form already at high temperatures above $\sim 800°$ C and are influenced during all stages of the cooling. Heating experiments and quantitative electron microscopy will solve some of these questions. So far we can only empirically use the size of c-domains to obtain information about the cooling history. Lally *et al.* (1972) recently found large c-domains in an An 93–95 anorthite from the Apollo 15 genesis rock (15415) and attribute it to the high Ca-content. From our evidence we conclude that the genesis rocks has to be a slowly cooled rock, similar to terrestrial metamorphic rocks or meteorites. This is very different from most other lunar rocks, such as 14310-basalt where the antiphase domains indicate relatively rapid cooling of an igneous rock. The differences between the two volcanic and the two plutonic specimens (missing of b-domains in the Japanese tuff compared with missing

c-domains in the lunar basalt and differences in size in meteoritic and metamorphic anorthites) may be partly caused by small variations in chemical composition.

The presence of submicroscopic structures in all plagioclase crystals raises the intriguing question how these features which are invisible in the light microscope are expressed in the optical properties. Antiphase domains, submicroscopical twins, exsolutions are likely to have some imprint on the orientation of the indicatrix and the fact that the optical state and the structural state not always conform (Wenk, 1968; Wenk and Nord, 1971) can possibly be explained as an influence of the microstructure.

References

Amelinckx, S.: The direct observation of dislocations. Solid State Phys., Suppl. 6 (1964).

Amelinckx, S.: The study of planar interfaces by means of electron microscopy. In: Modern diffraction and imaging techniques in materials science (S. Amelinckx, R. Gevers, G. Remaut, J. Van Landuyt, eds), p. 257–294. Amsterdam-London: North-Holland Publ. Co. 1970.

Appleman, D. E., Nissen, H.-U., Stewart, D. B., Clark, J. R., Dowty, E., Huebner, J. S.: Studies of lunar plagioclases, tridymite and cristobalite. Proc. Second Lunar Sci. Conf. Geochim. Cosmochim. Acta, Suppl. 2, vol. 1, p. 117–133. Cambridge, Massachusetts and London, England: The MIT Press 1971.

Barber, D. J.: Thin foils of non-metals made for electron microscopy by sputter-etching. J. Mat. Sci. 5, 1–8 (1970).

Brown, W. L., Hoffmann, W., Laves, F.: Über kontinuierliche und reversible Transformationen des Anorthits ($CaAl_2Si_2O_8$) zwischen 25 und 350° C. Naturwissenschaften 50, 221 (1963).

Bruno, E., Gazzoni, G.: Ricerche roentgenografiche su plagioclasi bytownitico-anortici tra 15° C e 1300° C. Periodico Mineral. (Rome) 36, 683–698 (1967).

Burri, C., Parker, R. C., Wenk, E.: Die optische Orientierung der Plagioklase. Basel und Stuttgart: Birkhäuser 1967.

Castaing, R.: Examen direct des métaux par transmission en microscopie et diffraction electronique. Rev. Métallurgie 52, 669–675 (1955).

Christie, J. M., Lally, J. S., Heuer, A. H., Fisher, R. M., Griggs, D. T., Radcliffe, S. V.: Comparative electron petrography of Apollo 11, Apollo 12 and terrestrial rocks. Proc. Second Lunar Sci. Conf. Geochim. Cosmochim. Acta, Suppl. 2, vol. 1, p. 69–89. Cambridge, Massachusetts, and London, England: The MIT Press 1971.

Cohen, J. B.: The order-disorder transformation. In: Phase transformations. Papers presented at a seminar of the American Society for Metals, October 12 and 13, 1968, p. 561–620. Metals Park, Ohio, American Society for Metals 1970.

Foit, F. F., Peacor, D. R.: High temperature diffraction data on selected reflections of an andesine and anorthite. Z. Krist. 125, 1–6 (1967).

Hirsch, P. B., Howie, A., Nicholson, R. B., Pashley, D. W., Whelan, M. J.: Electron microscopy of thin crystals. London: Butterworths 1965.

Kempster, C. J. E., Megaw, H. D., Radoslovich, E. W.: The structure of anorthite, $CaAl_2Si_2O_8$. I. Structure analysis. Acta Cryst. 15, 1005–1017 (1962).

Kôzu, S.: Optical, chemical and thermal properties of anorthite from three localities in
    Japan. Sci. Rep. Tohoku Imp. Univ. [Ser. 2], II, 8–33 (1914).
Lally, S., Fisher, R. M., Christie, J. M., Griggs, D. T., Heuer, A. H., Nord, G. L., Jr., Radcliffe,
    S. V.: Electron petrography of Apollo 14 and 15 samples. 3. Lunar Science Conf., Houston
    (1972).
Laves, F., Czank, M., Schulz, H.: The temperature dependence of the reflection intensities
    of anorthite ($CaAl_2Si_2O_8$) and the corresponding formation of domains. Schweiz. Mineral.
    Petrog. Mitt. 50, 519–525 (1970).
Laves, F., Goldsmith, J. R.: Polymorphism, order, disorder, diffusion and confusion in the
    feldspars. Estud. Geologicos, Cursillos y Conferencias, No. 8, 71–80 (1961).
Laves, F., Goldsmith, J. R.: The effect of temperature and composition on the Al—Si
    distribution in anorthite. Z. Krist. 106, 227–235 (1955).
Leisen, E.: Beitrag zur Kenntnis der Dispersion der Kalknatronfeldspäte. Z. Krist. 89, 49–79
    (1934).
Loewenstein, W.: The distribution of aluminium in the tetrahedra of silicates and aluminates.
    Am. Mineralogist 39, 92–96 (1954).
Marcinkowski, M. J.: Theory and direct observation of antiphase boundaries and dislocations
    in superlattices. In: Electron microscopy and strength of materials (G. Thomas and
    J. Washburn, eds.), p. 333–440. New York-London: Interscience Publishers 1963.
McConnell, J. D. C., Fleet, S. G.: Direct electron-optical resolution of antiphase domains in a
    silicate. Nature (Lond.) 199, 586 (1963).
Megaw, H. D.: Order and disorder in feldspars. Norsk Geol. Tidsskr. 42, No. 2, 104–137 (1962).
Nissen, H. U., Bollmann, W.: Submicroscopic fabrics in feldspars. Electron Microscopy 1966,
    Vol. 1, 591–592 (1966).
Radcliffe, S. V., Heuer, A. H., Fisher, R. M., Christie, J. M., Griggs, D. T.: High voltage (800 kV)
    electron petrography of type B rock from Apollo 11. Proc. Apollo 11 Lunar Sci. Conf.
    1, 731–748 (1970).
Ribbe, P. H.: Observations on the nature of unmixing in peristerite plagioclases. Norsk. Geol.
    Tidsskr. 42, No. 2, 138–151 (1962).
Ribbe, P. H., Colville, A. A.: Orientation of the boundaries of out-of-step domains in anorthite.
    Mineral. Mag. 36, 814–819 (1968).
Smith, J. V., Ribbe, P. H.: Atomic movements in plagioclase feldspars. Contr. Mineral. and
    Petrol. 21, 157–202 (1969).
Thomas, G.: Transmission electron microscopy of metals. New York: Wiley 1962.
Ulbrich, M.: Systematics of eucrites and howardite meteorites and a petrographic study of
    representative individual eucrites. M. A. thesis, University of California, Berkeley, 1971.
Warlimont, H.: The order-disorder transformation. Discussion. In: Phase transformations.
    Papers presented at a seminar of the American Society for Metals, October 12 and 13,
    1968, p. 621–624. Metals Park, Ohio, American Society for Metals 1970.
Wainwright, J. E., Starkey, J.: A refinement of the structure of anorthite. Z. Krist. 133,
    75–80 (1971).
Wenk, E.: Das reaktivierte Grundgebirge der Zentralalpen. Geol. Rundschau 52, 754–766
    (1962).
Wenk, H. R.: Submicroscopical twinning in lunar and experimentally deformed pyroxenes.
    Contr. Mineral. and Petrol. 26, 315–323 (1970).
Wenk, H. R.: Geologische Beobachtungen im Bergell. I. Gedanken zur Genese des Bergeller
    Granits. Rückblick und Ausblick. Schweiz. Mineral. Petrog. Mitt. 50, 321–348 (1970).
Wenk, H. R., Nord, G. L.: Lunar bytownite from sample 12032,44. Proc. Second Lunar
    Sci. Conf., Geochim. Cosmochim. Acta, Suppl. 2, vol. 1, p. 135–140. Cambridge, Massa-
    chusetts, and London, England: The MIT Press 1971.
Wenk, H. R., Ulbrich, M., Müller, W. F.: Lunar plagioclase (A mineralogical study). 3. Lunar
    Science Conf., Houston (1972).

Dr. W. F. Müller   Prof. H. R. Wenk
Department of Materials Science   Department of Geology and Geophysics
and Engineering   University of California
University of California   Berkeley, California 94720, U.S.A.
Berkeley, California 94720, U.S.A.

Four new structure refinements of olivine

By H.-R. WENK

Department of Geology and Geophysics and Space Sciences Laboratory
University of California at Berkeley

and K. N. RAYMOND

Department of Chemistry, University of California at Berkeley

Auszug

Mg/Fe-Ordnung in Olivin wurde von FINGER (1969/70) auf Grund von Röntgendaten vorgeschlagen und mit Mössbauer-Spektren (BUSH et al., 1970) bewiesen. Neue Strukturverfeinerungen an vier magnesiumreichen Olivinen ergaben Werte für Extinktionskoeffizienten, Atomlagen, anisotrope Temperaturfaktoren, Mg/Fe-Verteilung und formale Ladungen mit zwei- bis zehnmal besserer Auflösung als bisher. Die Parameter wurden mit der Methode der kleinsten Quadrate von Röntgendaten verfeinert unter Berücksichtigung der Einschränkungen durch chemische Zusammensetzung und elektrostatische Neutralität auf die Ableitungen. R-Werte liegen zwischen 2% und 3%. Mondproben zeigen signifikante (20 Standardabweichungen) Ordnung von Fe auf der kleineren M(1)-Lage [52% Fe auf M(1), 48% auf M(2)], metamorphe Forsterite sind grundsätzlich ungeordnet. Formale Ladungen wurden bestimmt: Fe,Mg $= +0,3$; Si $= +0.2$ und O $= -0,2$. Der Extinktionskoeffizient, ein empfindliches Maß für strukturelle Defekte, ist viel kleiner für Proben aus dem Mondstaub, die Strahlungsschäden und Wirkungen von Stoßwellendeformation zeigen, als für die metamorphen Forsterite. Mittlere M(1)—O- und M(2)—O-Abstände nehmen linear mit dem Fe/(Fe + Mg)-Quotienten zu.

Abstract

Mg/Fe order in olivine has been suggested from x-ray data (FINGER, 1969/70) and proven with Mössbauer spectra (BUSH et al., 1970). New structure refinements on four magnesium-rich olivines give two to ten times improved values for extinction coefficients, atomic positions, anisotropic temperature factors, site occupancies, and formal charges. The parameters have been refined from x-ray data by least-squares methods imposing proper constraints of chemical composition and electrostatic neutrality on derivatives. R factors range be-

tween 2 and 3%. Lunar samples show significant (twenty standard deviations) order of Fe on the smaller M(1) site [52% Fe on M(1), 48% Fe on M(2)], metamorphic forsterites are essentially disordered. Formal charges have been determined: Fe, Mg = +0.3, Si = +0.2, O = −0.2. The extinction coefficient, a sensitive measure for structural defects, is much lower for specimens from lunar dust, which show radiation damage and possible effects of shock deformation. Mean M(1)—O and M(2)—O distances increase linearly with Fe/(Fe + Mg).

Introduction

BRAGG and BROWN (1926) determined the basic structure of olivine and found hexagonal close packing of oxygen with Mg and Fe occupying half of the distorted octahedral interstices [the M(1) and M(2)
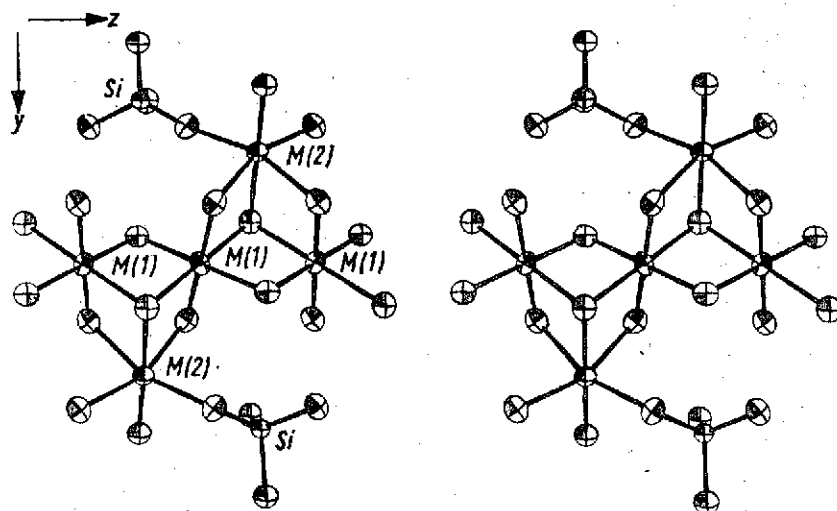
Fig. 1. Stereoscopic pair of drawings showing the crystal structure of olivine (Yosemite forsterite). The ellipsoids represent 99% probability contours of thermal motion. z axis is horizontal, y axis vertical, view is along x

sites], and Si occupying one-eighth of the tetrahedral interstices [the T site], see Fig. 1. Structures of olivines of different compositions have been refined, with emphasis on the determination of structural variations in this Mg-Fe solid solution series. Until recently, however, no deviations from ideal substitution have been found (BELOV et al., 1951; BORN, 1964; HANKE and ZEMANN, 1963; HANKE, 1963; BIRLE et al., 1968). ELISEEV (1958) reported deviations of the lattice parameters from VEGARD's rule in the fayalite-forsterite solid

solution series, which was probably based on inaccurate chemical data. GHOSE (1962) predicted that Fe would preferentially occupy the larger M(2) site, in analogy to orthopyroxenes. These suggestions and the fact that in isostructural compounds like monticellite, $CaMgSiO_4$ (ONKEN, 1965), and glaucochroite, $CaMnSiO_4$ (CARON et al., 1965), the cations are ordered encouraged other investigators to continue the search for order in olivines. It has been the stimulus of the moon that has led several crystallographers independently to refine structures of lunar olivines to determine if the Fe/Mg distribution can be used as an indicator for the geological history of these important minerals, which occur in many different rocks and which have been formed under very different geological conditions.

Partial order was first suggested from spectroscopic measurements (BURNS, 1969; BUSH et al., 1970) but the results were not conclusive (BURNS, 1970). The latest development of x-ray single-crystal diffractometers has improved the quality of x-ray data and thus enhances the resolution of a standard crystal-structure refinement. It becomes possible to determine electron densities in fractions of an electron. The refinements of FINGER (1969/70, 1971) suggest preference of Fe on the M(1) site in igneous olivines, with deviations from disorder of a few standard deviations. BROWN (1971) describes small order, which they think is insignificant. In their high-temperature experiments they find an increasing distortion of the M(1) site with increasing temperature. With this background in mind, and with the need to obtain data on lunar crystals, the present investigation has been started. The aim was to push the resolution of a refinement to its limits to determine if order in igneous olivines is real. This paper consists of two equally important parts: The first part discusses in some detail the influence of more than one dependent and independent constraint of the occupancy factors on the derivatives in the least-squares refinement. So far, only a single constraint has been taken into account in the refinement of mineral structures (FINGER, 1967). The second part presents the results of four crystal-structure refinements and tries to demonstrate that these results are not experimental artifacts. FINGER's results have been confirmed. There exists small but significant order in chemically intermediate olivines. Yet it has not been possible to resolve the olivine controversy (the question whether the thermal history affects the Fe/Mg distribution), and more structural work should be done on geologically well-defined olivines.

Experimental procedure

Data collection

Small crystals (0.1—0.2 mm) of isometric shape were selected from
various rock specimens; two are metamorphic forsterites and two are
intermediate (Fa 30) olivines from lunar basalt. Specifications are
given in Table 1. The crystals were first checked on a precession
camera for space group, domain structure, and asterism. For all of
them, the space group *Pbnm* was determined. No extra reflections
have been observed (ELISEEV, 1958). Then the crystals were oriented
on a computer-controlled Picker diffractometer. From the positions
of twelve reflections, the lattice constants and the orientation angles

Table 1. *General information about the olivines investegated*

Specimen number	Source	Mineralogical description
103—481	Yosemite 1-1/2 miles southwest May Lake	brucite-forsterite-humite-spinel-calcite marble
Sci 59	Bergell Alps Road cut Casalic 1160 m, Bondo-Ceresc	amphibole-orthopyroxene-chlorite olivinite, recrystallized
12070—12.4	Oceanus Procellarum Apollo 12	fine lunar dust, single crystal
10085	Mare Tranquillitatis Apollo 11	coarse fines, plagioclase-pyroxene-ilmenite-olivine basalt

were refined by least squares (Table 2). They agree closely (Fig. 2),
but not perfectly, with the determinative curves of YODER and
SAHAMA (1957), JAMBOR and SMITH (1964), and JAHANBAGLOO (1969).
Data were collected by the θ-2θ scan technique up to Bragg angles
of 100° using monochromatic Mo$K\alpha$ radiation, with highly oriented
graphite used as the monochromator crystal. The 2θ scan width was
1.4° + $\Delta2\theta$ where $\Delta2\theta$ is the distance between the calculated maxima
for the $K_{\alpha1}$ and $K_{\alpha2}$ peaks. The scanning rate was 1 degree per minute
with 10-second stationary background counts on either side of the scan.
Standard deviations of individual reflections were determined from

Table 2. *Lattice constants of olivines (Pbnm setting)*

Lattice constants	Yosemite 103—481	Bergell Alps Sci 59	Oceanus Procellarum Apollo 12 12070—12.4	Mare Tranquillitatis Apollo 11 10085
a	4.7533(5)[1]	4.7623(4)	4.7748(5)	4.7768(6) Å
b	10.1972(7)	10.2284(11)	10.2798(16)	10.2943(16) Å
c	5.9821(3)	5.9942(6)	6.0087(9)	6.0174(9) Å

[1] In this and the following tables standard deviations in the least significant digits are given in parentheses.

Table 3. *X-ray data collection*

Parameter data	Yosemite 103—481	Bergell Alps Sci 59	Oceanus Procellarum Apollo 12 12070-12.4	Mare Tranquillitatis Apollo 11 10085
Crystal size	0.15 × 0.15 × 0.15mm	0.15 × 0.10 × 0.10mm	0.2 × 0.15 × 0.1mm	0.3 × 0.2 × 0.2mm
Linear absorption coefficient μ	11	19	40	45 cm^{-1}
Total number of observations	1427	3644	2349	3161
Number of independent observations	1125	1797	1321	2029
Number of independent reflections used in refinement ($|F|^2 > 3\sigma$)	783	851	882	1459
R factor (all data)	0.023	0.022	0.022	0.022
Weighted R (all data)	0.032	0.026	0.029	0.032

counting statistics of integrated count and background (DUESLER and RAYMOND, 1971). An additional error of 3% of the net intensity was added to the standard deviation to avoid overweighting of intense

reflections. The raw intensities were corrected for Lorentz and polarization effects. An absorption correction was not found to be necessary because intensities of equivalent reflections were not significantly

Table 4. *Chemical composition of olivines*

(microprobe analyses)

	Yosemite 103—481	Bergell Alps Sci 59	Oceanus Procellarum Apollo 12 12070-12.4	Mare Tranquillitatis Apollo 11 10085[1]
Weight percent				
SiO_2	42.21%	~ 37.79%	37.10%	36.88%
FeO	1.21	9.25	27.53	26.37
TiO_2	—			
MnO	0.29	0	0	0
NiO	traces	0.74	0.37	0
MgO	56.03	49.30	34.17	35.95
CaO	0.06	0.02	0.35	0.36
Na_2O	—			
Total	99.80	97.1	99.52	99.56
Formula used in refinement				
Fe	0.012	0.099	0.319	0.300[2]
Mn	0.003	—	—	—
Ni	0	0.008	0.004	0
Mg	0.985	0.893	0.672	0.695
Ca	< 0.001	0	0.005	0.005
Si	0.5	0.5	0.5	0.5
O	2	2	2	2
Refined formula from x-ray data				
Fe				0.358(5)
Mg				0.637
Ca				0.005

(Fe, Mn, Ni, Mg, Ca values for Yosemite are braced together as 1.)

[1] Chemical analysis done on different crystal from the same rock.

[2] Later replaced by formula below.

different. Intensities of equivalent reflections were averaged. Systematic extinctions were rejected. A new standard deviation of the averaged intensity was calculated. The larger one (counting statistic averaging) was used as weight in the least-squares refinement. More

information about the specimens data collection and data processing is given in Table 3. After the data collection, the crystals were chemically analyzed with the microprobe (Table 4). During this procdeure the Apollo 11 crystal was lost and the analysis was done on another crystal from the same rock. This crystal apparently did not have an identical composition, which was readily seen in aberrant electrical charges for Si. The final Fe/Mg ratio was therefore refined from the x-ray data.

Least-squares refinement

The refinement of the structure was done with a modified version of the Busing-Levy least-squares program (BUSING et al., 1962). Atomic scattering factors were interpolated from the table of CROMER and MANN (1968). Real and imaginary anomalous scattering factors were used for Fe (CROMER, 1965). Several assumptions for the structure model were made: a) there are no vacancies; b) traces of Mn and Ni are closely related to iron, and the atomic scattering factors were adjusted accordingly; c) all Ca is on the M(2) site in analogy to monticellite; d) the overall electrical charge is zero; e) all oxygen has equal charge; f) the degree of ionization of Fe and Mg is equal; g) atomic scattering factors for neutral atoms were used. All refined parameters are relatively insensitive to each of these assumptions. Errors in the chemical analysis (Fe/Mg ratio) are mainly expressed in the refined electrical charge and not in the Fe/Mg distribution. The 44 positional, thermal and scale parameters which were refined imposing proper constraints on the derivatives are: a) atomic coordinates of M(2), Si, O(1), O(2), and O(3); b) anisotropic temperature factors for all atoms; c) scale factors for Fe(1), Fe(2), and Si to calculate the Fe/Mg distribution and an approximated ionic charge; d) an overall isotropic extinction factor (ZACHARIASEN, 1968). After a few cycles the refinement converged with R values of 2—3%.

The least-squares refinement of site occupancies has to take into account constraints imposed by the chemical composition, the lattice geometry, and overall electrostatic neutrality. If many independent and correlated constraints are acting, then the effect on the derivatives is no longer trivial. We think that the best way to explain the procedure to the reader is to specify explicitly for each refinement all the variables and constraints. This specification, which permits an evaluation of the refinement procedure, is done most compactly in matrix notation. RAYMOND (1972) derived the formal solution of the

general problem. A crystal has n atoms, and each atom has a multiplicity factor a_i. We cannot refine all of these multiplicity factors because of constraints. If there are n atoms and m linear equations of constraint, then there are only $k = n - m$ independent variables, V_k. We form a square matrix, Q, by combining independent variables with the constraints. In the following discussion, variables and constraints are specified for each crystal. For the *Yosemite forsterite* with very little Fe, the refinement has been done on the basis of the formula $(Mg,Fe)SiO_4$ with six atoms [M(1), M(2), Si, O(1), O(2), O(3)]. Occupancies of M(1), M(2), and Si were refined, thus the matrix becomes

$$
Q = \begin{bmatrix}
1 & 0 & 0 & 0 & 0 & 0 \\
0 & 1 & 0 & 0 & 0 & 0 \\
0 & 0 & 1 & 0 & 0 & 0 \\
12.303 & 12.203 & 14 & 8 & 8 & 8 \\
0 & 0 & 0 & 1 & -1 & 0 \\
0 & 0 & 0 & 2 & 0 & -1
\end{bmatrix}
\begin{bmatrix}
a_{(M)1} \\
a_{(M)2} \\
a_{Si} \\
a_{(O)1} \\
a_{(O)2} \\
a_{(O)3}
\end{bmatrix}
=
\begin{bmatrix}
V_1 \\
V_2 \\
V_3 \\
C_1\,[35.203] \\
C_2\,[0] \\
C_3\,[0]
\end{bmatrix}
$$

The first constraint, C_1, ensures that electrostatic neutrality is maintained. The number of electrons of the neutral metal atom (Mg, corrected for traces of Fe and Mn) is 12.203. Constraints C_2 and C_3 impose equal occupancy on the oxygen sites. From the refined occupancies, an approximate formal electrical charge, q, can be calculated:

$$
q = \frac{Z\,(a_i^0 - a_i)}{a_i} \, ,
$$

where a_i^0 is the occupancy in the chemical formula, and a_i is the refined occupancy. The atomic number of the element is Z. This refinement of the charge from a constant scale factor is not strictly true because the scattering-factor curve for an ionized atom is not proportional to that of a neutral atom. The two curves differ mostly at low diffraction angles and almost coincide at high angles. But as scale factors are mainly determined by low-angle reflections and because charges were very small, it was found sufficient to use scattering-factor tables for neutral atoms and to refine a scale factor. It would be more accurate to interpolate a new scattering-factor table after each cycle of the refinement. Yet this raw treatment of charges is certainly better than ignoring them and produces very reasonable results. Notice that, due to the refinement of the electrical charge, the occupancy of oxygen, a_O, in the second and third constraint equations is not constant.

In the case of the *Bergell olivine* (Sci 59) the relation is more complicated. There is now sufficient Fe to separate the M sites into an Fe and an Mg contribution. Traces of other transition elements (e.g. Ni, Mn) are combined with the chemically similar Fe. The formula is $Fe_{0.107}Mg_{0.893}SiO_4$ with eight atoms [Fe(1), Fe(2), Si, Mg(1), Mg(2), O(1), O(2), O(4)]. Occupancies of Fe(1), Fe(2), and Si were refined and two additional constraints were introduced. The first constraint imposes equal occupancy of M(1) and M(2), and C_2 introduces the Fe/Mg ratio obtained from the chemical analysis. Formal charges, q, were taken into account. The equations are no longer strictly linear and were reset for q after every cycle in the refinement.

$$
Q = \begin{bmatrix}
1 & 0 & 0 & 0 & 0 & 0 & 0 & 0 \\
0 & 1 & 0 & 0 & 0 & 0 & 0 & 0 \\
0 & 0 & 1 & 0 & 0 & 0 & 0 & 0 \\
b_1 & -b_1 & 0 & b_2 & -b_2 & 0 & 0 & 0 \\
b_1 & b_1 & 0 & -b_2 \cdot \frac{Fe}{Mg} & -b_2 \cdot \frac{Fe}{Mg} & 0 & 0 & 0 \\
26.134 & 26.134 & 14 & 12.0 & 12.0 & 8 & 8 & 8 \\
0 & 0 & 0 & 0 & 0 & -1 & 1 & 0 \\
0 & 0 & 0 & 0 & 0 & -2 & 0 & 1
\end{bmatrix}
\begin{bmatrix}
a_{Fe(1)} \\ a_{Fe(2)} \\ a_{Si} \\ a_{Mg(1)} \\ a_{Mg(2)} \\ a_{O(1)} \\ a_{O(2)} \\ a_{O(3)}
\end{bmatrix}
=
\begin{bmatrix}
V_1 \\ V_2 \\ V_3 \\ C_1[0] \\ C_2[0] \\ C_3[36.50] \\ C_4[0] \\ C_5[0]
\end{bmatrix}
$$

where $b_1 = \dfrac{26.134 + q}{26.134}$, $b_2 = \dfrac{12.0 + q}{12.0}$, and Fe/Mg $= 0.1198$.

The lunar samples *Apollo 11* and *Apollo 12* contain enough Ca to treat it as a separate atom. In the isostructural monticellite ($CaMgSiO_4$), Ca is ordered on the M(2) site (ONKEN, 1965) and it was placed there by analogy. For Apollo 11 the formula is $Fe_{0.300}Mg_{0.695}Ca_{0.004}SiO_4$; and for Apollo 12 it is $Fe_{0.323}Mg_{0.672}Ca_{0.004}SiO_4$ with nine atoms: the same independent variables were used as before.

$$
Q = \begin{bmatrix}
1 & 0 & 0 & 0 & 0 & 0 & 0 & 0 & 0 \\
0 & 1 & 0 & 0 & 0 & 0 & 0 & 0 & 0 \\
0 & 0 & 1 & 0 & 0 & 0 & 0 & 0 & 0 \\
+b_1 & -b_1 & 0 & b_2 & -b_2 & -1 & 0 & 0 & 0 \\
b_1 & b_1 & 0 & -b_2 \cdot \frac{Fe}{Mg} & -b_2 \cdot \frac{Fe}{Mg} & 0 & 0 & 0 & 0 \\
0 & 0 & 0 & 0 & 0 & 1 & 0 & 0 & 0 \\
\begin{matrix}26.0(11) & 26.0 \\ 26.015(12) & 26.015\end{matrix} & & 14 & 12 & 12 & 20 & 8 & 8 & 8 \\
0 & 0 & 0 & 0 & 0 & 0 & \bar{1} & 1 & 0 \\
0 & 0 & 0 & 0 & 0 & 0 & \bar{2} & 0 & 1
\end{bmatrix}
\begin{bmatrix}
a_{Fe(1)} \\ a_{Fe(2)} \\ a_{S} \\ a_{Mg(1)} \\ a_{Mg(2)} \\ a_{Ca(2)} \\ a_{O(1)} \\ a_{O(2)} \\ a_{O(3)}
\end{bmatrix}
=
\begin{bmatrix}
V_1 \\ V_2 \\ V_3 \\ C_1[0] \\ C_2[0] \\ C_3[0.005] \\ C_4 {[39.240] \atop [39.566]} \\ C_5[0] \\ C_6[0]
\end{bmatrix}
$$

with $b_1 = \dfrac{26 + q}{26}$, $b_2 = \dfrac{12 + q}{12}$, and Fe/Mg = 0.4317 for Apollo 11

and $b_1 = \dfrac{26.015 + q}{26.015}$, $b_2 = \dfrac{12 + q}{12}$, and Fe/Mg = 0.4927 for Apollo 12.
The refinements were done weighing the reflections indirectly proportional to their standard deviation. To check the quality of the data,
the final cycles have also been done with unit weights for all reflections.
The results agreed within one or two standard deviations.

Table 5. *Atomic parameters of olivine*

	Yosemite 103—481	Bergell Alps Sci 59	Oceanus Procellarum Apollo 12 12070-12.4	Mare Tranquillitatis Apollo 11 10085
M(1) $x = y = z = 0$				
M(2)				
x	0.99119(10)	0.98968(8)	0.98765(7)	0.98724(5)
y	0.27744(4)	0.27772(4)	0.27821(3)	0.27842(2)
$z = 1/4$				
Si				
x	0.42625(7)	0.42681(7)	0.42752(7)	0.42786(5)
y	0.09409(4)	0.09443(4)	0.09521(4)	0.09535(3)
$z = 1/4$				
O(1)				
x	0.76557(20)	0.76589(18)	0.76603(19)	0.76645(13)
y	0.09144(9)	0.09148(9)	0.09185(9)	0.09211(7)
$z = 1/4$				
O(2)				
x	0.22163(20)	0.22066(19)	0.21720(20)	0.21690(14)
y	0.44721(8)	0.44767(8)	0.44882(8)	0.44930(6)
$z = 1/4$				
O(3)				
x	0.27723(12)	0.27838(13)	0.28034(13)	0.28122(9)
y	0.16311(6)	0.16333(6)	0.16381(6)	0.16406(5)
z	0.03315(11)	0.03329(10)	0.03431(10)	0.03422(8)

Table 6. *Site occupancies and apparent charges of olivines*

	Yosemite 103—481	Bergell Alps Sci 59	Oceanus Procellarum Apollo 12 12070-12.4	Mare Tranquillitatis Apollo 11 10085
Occupancies				
M(1)				
Fe	0.006(3)	0.0526(6)	0.1672(6)	0.1871(7)
Mg	0.494	0.4474	0.3328	0.3129
M(2)				
Fe	0.009(4)	0.0541(6)	0.1558(4)	0.1709(7)
Mg	0.491	0.4459	0.3392	0.3241
Ca	—	—	0.005	0.005
K_D	[0.66(20)]	0.969(24)	1.096(10)	1.134(11)
Charges per atom				
M(1) = M(2)	+ 0.33(3)	+ 0.22(3)	0.34(4)	0.13(5)
Si	+ 0.27(3)	+ 0.20(8)	+ 0.03(3)	0.14(3)
O(1) = O(2) = O(3)	— 0.23	— 0.15	— 0.18	— 0.10
Extinction coefficient	$0.90(4) \cdot 10^{-6}$	$2.94(11) \cdot 10^{-6}$	$0.15(4) \cdot 10^{-6}$	$0.27(2) \cdot 10^{-6}$

Table 7. *Thermal parameters of olivines* ($\beta \times 10^5$)

{Temperature factors are of the form $\exp [-(\beta_{11}h^2 + \beta_{22}k^2 + \beta_{33}l^2 + 2\beta_{12}hk + 2\beta_{13}hl + 2\beta_{23}kl)]$}

	Yosemite 103—481	Bergell Alps Sci 59	Oceanus Procellarum Apollo 12 12070-12.4	Mare Tranquillitatis Apollo 11 10085
M(1)				
β_{11}	333(15)	287(12)	498(10)	417(6)
β_{22}	140(3)	110(3)	162(3)	147(2)
β_{33}	316(10)	214(8)	204(7)	347(4)
β_{12}	— 9(5)	0(5)	— 4(3)	— 5(2)
β_{13}	—43(9)	—40(7)	—36(5)	—45(3)
β_{23}	—34(5)	—36(4)	—41(3)	—41(2)
M(2)				
β_{11}	418(17)	470(14)	692(13)	585(7)
β_{22}	99(4)	69(3)	106(2)	94(1)
β_{33}	375(11)	269(8)	240(7)	365(4)
β_{12}	9(6)	2(5)	14(4)	2(2)
$\beta_{13} = \beta_{23} = 0$				

Table 7. *(Continued)*

	Yosemite 103—481	Bergell Alps Sci. 59	Oceanus Procellarum Apollo 12 12070-12.4	Mare Tranquillitatis Apollo 11 10085
Si				
β_{11}	178(12)	133(11)	340(11)	257(7)
β_{22}	88(3)	56(2)	99(2)	89(2)
β_{33}	284(8)	179(6)	172(7)	301(5)
β_{12}	2(4)	4(4)	9(4)	13(2)
$\beta_{13} = \beta_{23} = 0$				
O(1)				
β_{11}	389(26)	238(24)	493(26)	369(14)
β_{22}	164(7)	145(6)	179(6)	172(3)
β_{33}	436(18)	329(16)	285(15)	431(11)
β_{12}	5(10)	11(11)	7(10)	15(6)
$\beta_{13} = \beta_{23} = 0$				
O(2)				
β_{11}	530(27)	501(27)	699(27)	619(17)
β_{22}	124(6)	84(6)	114(5)	103(3)
β_{33}	466(18)	326(16)	358(15)	463(11)
β_{12}	2(11)	10(10)	4(11)	—12(6)
$\beta_{13} = \beta_{23} = 0$				
O(3)				
β_{11}	514(19)	445(17)	634(19)	576(12)
β_{22}	172(5)	127(4)	182(4)	161(3)
β_{33}	445(13)	326(11)	320(11)	445(8)
β_{12}	1(8)	24(7)	13(7)	25(5)
β_{13}	—22(13)	—15(12)	—25(11)	—10(8)
β_{23}	45(6)	54(5)	70(5)	66(4)

Results

The refined parameters are listed in Tables 5, 6, and 7. We will discuss briefly the significance and importance of these results. Standard deviations are especially low for the Apollo 11 olivine, where 1459 independent reflections have been used in the refinement.

Atomic positions

From atomic positions selected interatomic distances were calculated (Table 8), and the important mean M(1)—O and M(2)—O distances are plotted in Fig. 2 as a function of the fayalite content.

Results of previous work are included. The new data show that both distances increase linearly with iron content. M(2)—O is about 0.03 Å larger than M(1)—O, and one might expect M(2) to be preferentially occupied by Fe, although the difference in size is quite small. A linear dependence is a reasonable physical assumption for an ideal ionic substitution. The strictly linear relation between calculated M—O
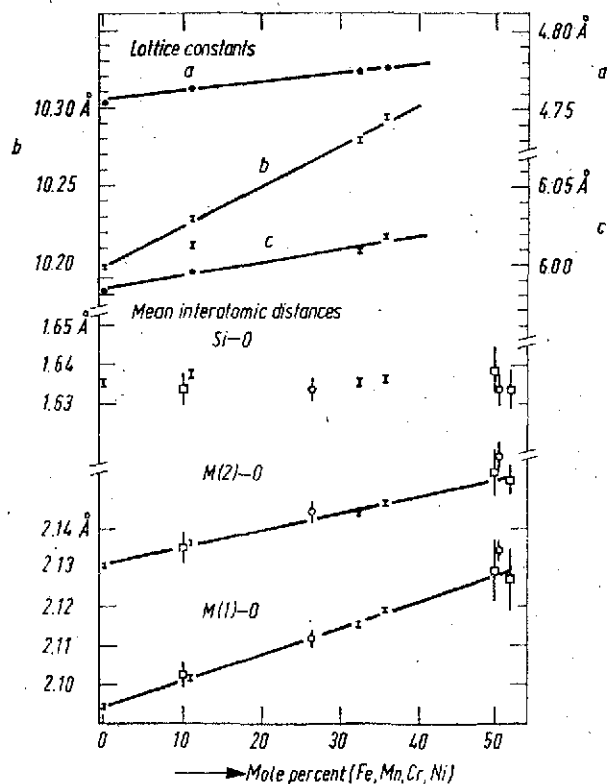

Fig. 2. Lattice constants and selected mean interatomic distances of olivines as a function of the iron content (error bars are rounded to 1—2 sigmas). □ BIRLE et al. (1968), ○ FINGER (1969/70), ● and ɪ this paper

distances and fayalite content within two standard deviations as documented by the four new data points is a good indication, although not a definite proof, that the standard deviation computed in the least-squares program is meaningful, and that the dependence, in fact, is linear. If either one of these assumptions were not true, it would be

Table 8. *Selected interatomic distances of olivines*

	Yosemite 103—481	Bergell Alps Sci 59	Oceanus Procellarum Apollo 12 12070-12.4	Mare Tranquillitatis Apollo 11 10085
Si tetrahedron				
1 Si—O(1)	1.6131(10) Å	1.6150(9) Å	1.6167(10) Å	1.6177(7) Å
1　　O(2)	1.6545(9)	1.6572(9)	1.6559(10)	1.6549(7)
2　　O(3)	1.6370(7)	1.6382(7)	1.6343(6)	1.6361(5)
mean	1.6354(8)	1.6372(8)	1.6353(7)	1.6362(6)
1 O(1)—O(2)	2.7434(13)	2.7445(13)	2.7360(14)	2.7371(20)
—O(3)	2.7577(10)	2.7600(6)	2.7577(10)	2.7580(8)
1 O(2)—O(3)[a]	2.5553(10)	2.5599(10)	2.5620(10)	2.5639(8)
1 O(3)—O(3)[a]	2.5945(13)	2.5980(13)	2.5920(12)	2.5968(11)
M(1) octahedron				
2 M(1)—O(1)	2.0851(6)	2.0891(6)	2.0967(7)	2.0992(5)
2　　—O(2)	2.0681(6)	2.0741(6)	2.0873(7)	2.0891(5)
2　　—O(3)	2.1313(6)	2.1420(6)	2.1610(7)	2.1678(5)
mean	2.0948(6)	2.1017(6)	2.1150(7)	2.1187(5)
2 O(1)—O(2)[b]	2.847(10)	2.854(10)	2.872(10)	2.873(8)
2　　—O(2)	3.0241(2)	3.0314(4)	3.0423(5)	3.0479(5)
2　　—O(3)[b]	2.8516(11)	2.8608(10)	2.8735(10)	2.8777(8)
2　　—O(3)	3.106(10)	3.118(10)	3.218(10)	3.151(8)
2 O(2)—O(3)[a]	2.5553(10)	2.5599(10)	2.5620(10)	2.5639(8)
—O(3)	3.3330(9)	3.3507(10)	3.3896(11)	3.3990(8)
M(2) octahedron				
1 M(2)—O(1)	2.1788(10)	2.1829(10)	2.1886(11)	2.1889(8)
1　　—O(2)	2.0487(10)	2.0571(9)	2.0682(10)	2.0731(7)
2　　—O(3)	2.2114(8)	2.2241(7)	2.2396(7)	2.2459(6)
2　　—O(3)	2.0666(7)	2.0639(7)	2.0624(7)	2.0601(5)
mean	2.1306(7)	2.1360(7)	2.1435(7)	2.1456(6)
2 O(1)—O(3)[b]	2.8516(11)	2.8608(10)	2.8735(10)	2.8777(8)
2　　—O(3)	3.0226(10)	3.0293(10)	3.0384(10)	3.0382(8)
2 O(2)—O(3)	3.1852(10)	3.1972(10)	3.2179(11)	3.2235(9)
2　　—O(3)	2.9320(9)	2.9341(9)	2.9343(10)	2.9357(7)
1 O(3)—O(3)[a]	2.5945(13)	2.5980(13)	2.5920(12)	2.5968(11)
2　　—O(3)	3.3876(13)	3.3962(13)	3.4167(13)	3.4206(11)
2　　—O(3)	2.9910(8)	2.9955(8)	3.0016(8)	3.0008(7)

[a] Edges shared between tetrahedron and octahedron.

[b] Edges shared between octahedra.

highly improbable that the error bars fall exactly on a straight line of all four data points. If the errors were artificially low, we would expect error bars to scatter outside the straight line in Fig. 3, as would be the case if smaller errors were assigned to the data points of BIRLE et al. (1968) and FINGER (1969/70).

Temperature factor

Anisotropic temperature factors have been refined for all atoms, imposing proper symmetry constraints. Numerical values are listed in Table 7. They are relatively small, larger for the lunar olivines than for the terrestrial forsterites. We attribute this to some structural defect, such as domain texture in the lunar crystals. Figure 1, where 99% probability contours are drawn for the Yosemite forsterite, shows a moderate anisotropy. Table 7 demonstrates that relative ratios of the temperature factors in all specimens are very consistent and therefore the anisotropy is certainly real.

Extinction coefficient

In the first stages of the refinement, large errors were found in the structure factors of strong low-angle reflections such as 004 (Yosemite forsterite: $F_{obs} = 98.5$, $F_{calc} = 130$) or 062 ($F_{obs} = 90$, $F_{calc} = 111$). Therefore, a correction for secondary extinction (ZACHA-RIASEN, 1968) was introduced in the refinement. The extinction coefficient varies by over an order of magnitude (Table 6). It is high for the re-crystallized metamorphic forsterites and low for lunar olivines, especially for a crystal from lunar dust (Apollo 11). Extinction from double diffraction is only large for very perfect crystals. We attribute the small extinction in lunar crystals to damage from cosmic and solar radiation. High track densities have been observed in many lunar minerals (e.g., ARRHENIUS et al., 1971; COMSTOCK et al., 1971; CROZAZ et al., 1971; FLEISCHER et al., 1970, 1971; PRICE and O'SULLIVAN, 1970). This type of damage seems more likely than tectonic defects (e.g. by meteorite impact) since asterism and bending is absent in precession photographs. The observation on these four olivines should not be generalized; i.e., the extinction coefficient certainly can not be used to distinguish between lunar and terrestrial olivines. It is quite likely that terrestrial olivine with structural defects also has a small extinction coefficient (FINGER, 1969/70). Notice that small extinc-

tion coefficients go parallel with large temperature factors, although there is no mathematical correlation between the two parameters. The temperature factor is a function of the Bragg angle and is mainly determined by high-angle reflections. The extinction coefficient is intensity-dependent and affects strong low-angle reflections. Absorption may change the extinction coefficient, although it equally affects strong and weak reflections. There is also no correlation between extinction coefficient and absorption in the four analyzed specimens.

Fe/Mg distribution

Table 6 lists occupancy factors for iron and magnesium on the $M(1)$ and $M(2)$ sites. From these occupancies a distribution coefficient K_D for the reaction $Fe(2) + Mg(1) \rightleftharpoons Mg(2) + Fe(1)$ is calculated,
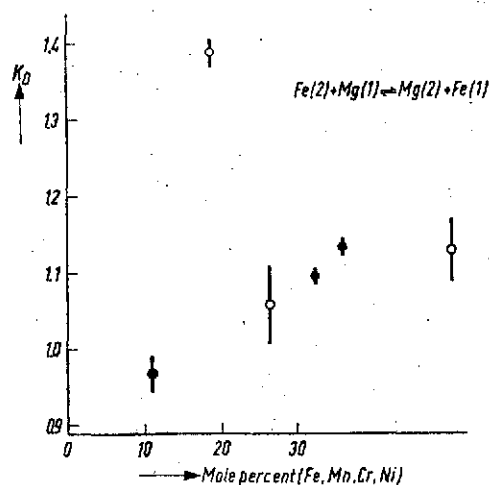

Fig. 3. Fe/Mg distribution coefficient K_D of several Mg-rich olivines as a function of the iron content (error bars are rounded to 1—2 sigmas). $K_D = \dfrac{Mg(2) \cdot Fe(1)}{Mg(1) \cdot Fe(2)}$.
○ Finger (1969/70, 1971), ● this paper

and K_D is plotted as a function of the fayalite content in Fig. 3. In metamorphic forsterites, Fe is essentially disordered. In olivines from lunar basalts there is small but significant (over 20 standard deviations) order of iron on the $M(1)$ site. The order of iron is about 5 percent, which is much smaller than 30 percent order, which has been determined from Mössbauer spectra (Bush et al., 1970; Virgo

et al., 1971). We believe that this small order is real for the following reasons:

1. Errors in the microprobe analyses of the Fe/Mg ratio are about one, at most 2 percent. But the chemical constraint is actually quite insensitive because Fe and Mg occupy the same sites and, regardless of the actual Fe/Mg ratio, the occupancy of the M(1) site in lunar olivines always refined to a heavier electron density of more than twenty standard deviations. Notice that Apollo 11 and 12 crystals gave quite similar results (although in the case of Apollo 12, the Fe/Mg ratio was refined from x-ray data).

2. Standard deviations obtained in the least-squares calculations are real. This is demonstrated for positional parameters by the linear correlation between M—O distances and the fayalite content for the four new data points (Fig. 2) and also by the fact that unit weighting of all reflections (an unrealistic model) shifted the results only 1—2 standard deviations. The latter argument is a good indication of high-quality data. With a perfect data set, the weighting scheme does not affect the results. If a weighting scheme reverses the order relations (BROWN, 1971) then the Fe/Mg distribution is beyond the resolution of the refinement or the weighting scheme is wrong.

3. Because of the large difference in scattering factors for Fe and Mg, small errors in the scattering factor table do not change the results appreciably. The same Fe/Mg distribution and the same *R* value were obtained using neutral or partially ionized atoms. In the present refinement, scale factors for Si and Fe(2) were refined in addition to Fe(1), which determines the Fe/Mg distribution. From these additional scale factors approximate charges have been calculated.

The extremely small Fe/Mg order in olivines suggests that the Fe/Mg distribution does not have a strong thermochemical significance. Order can be only detected satisfactorily in chemically intermediate olivines. These are very rare except in some igneous rocks and therefore the geological importance of Fe/Mg order in olivines is small. Yet we tend to agree with FINGER (1969/1970, 1971)—although the present data are not yet conclusive—that in olivines which crystallize from a hot magma ($\sim 1200\,°C$) Fe preferentially occupies the M(1) site. In the metamorphic forsterites, crystallizing at 500—700 °C, order is very small and, if existent, Fe may be enriched on the larger M(2) site.

Electrical charge

The refinement of formal charges affects other parameters insignificantly and barely changes the R value. The results in Table 6 indicate for $Fe = Mg^+ + 0.20$ to 0.30, for Si^+ 0.10 to 0.20, and for O^- 0.10 to 0.20. This is about 5 to 10 percent of the charge of the fully ionized ion. The relatively small actual charge indicates that covalent bonding plays an important role in the olivine structure. We expect that a similar magnitude of formal charges will be found in all silicates and oxides. Because the charges are so small, a good approximation is obtained by applying a constant scale factor to each scattering-factor table for neutral atoms, as discussed above. The refined charges immediately indicate errors in the chemical formula. The value and the standard deviation of the refined charge is a good measure of the resolution of the refinement and will be even more so if we have more data with which to compare it. The introduction of the electrical charge as a variable in the least-squares refinement requires, however, a formal treatment of the various constraints as has been outlined above.

Acknowledgments

References

G. ARRHENIUS, S. LIANG, D. MacDOUGALL, L. WILKENING, N. BAHANDARI, S. BHAT, D. LAL, G. RAJAGOPALAN, A. S. TAMHANE, V. S. VENKATAVARADAN (1971), The exposure history of the Apollo 12 regolith. Proc. Second Lunar Science Conf. Vol. 3, 2583—2598.

N. V. BELOV, E. N. BELOVA, N. H. ANDRIANOVA, and P. F. SMIRNOVA (1951), Determination of the parameters in the olivine (forsterite) structure with the harmonic three-dimensional synthesis. Dokl. Akad. Nauk SSSR. 81, 399—402.

J. D. BIRLE, G. V. GIBBS, P. B. MOORE, and J. V. SMITH (1968), Crystal structures of natural olivines. Amer. Mineral. 53, 807—824.

L. BORN (1964), Eine „gitterenergetische Verfeinerung" der freien Mg-Position im Olivin. Neues Jahrb. Mineral., Monatsh. 81—94.

W. L. BRAGG und G. B. BROWN (1926), Die Struktur des Olivins. Z. Kristallogr. 63, 538—556.

G. BROWN (1971), Order-disorder in olivine. Conf. on petrologic crystal chemistry, AGU. Edgartown, Mass.

R. G. BURNS (1969) Evidence for cation ordering in olivine minerals from crystal field spectra (abstract). Acta Crystallogr. A 25, 559.

R. G. BURNS (1970), Crystal field spectra and evidence of cation ordering in olivine minerals. Amer. Mineral. 55, 1608—1632.

W. R. BUSH, S. S. HAFNER, and D. VIRGO (1970), Some ordering of iron and magnesium at the octahedrally coordinated sites in a magnesium-rich olivine. Nature [London] 227, 1339—1341.

W. R. BUSING, K. O. MARTIN, and H. A. LEVY (1962), ORFLS, a FORTRAN crystallographic function and error program. ORNL-TM-305.

L. G. CARON, R. P. SANTORO, and R. E. NEWNHAM (1965), Magnetic structure of CaMnSiO₄. J. Physics Chem. Solids 26, 927—930.

G. M. COMSTOCK, A. O. EVWARAYE, R. L. FLEISCHER, and H. R. HART, Jr. (1971), The particle track record of lunar soil. Proc. Second Lunar Science Conf. Vol. 3, 2569—2582.

D. T. CROMER (1965), Anomalous dispersion corrections computed from self-consistent field relativistic Dirac-Slater wave functions. Acta Crystallogr. 18, 17—23.

D. T. CROMER and J. B. MANN (1968), X-ray scattering factors computed from numerical Hartree-Fock wave functions. Acta Crystallogr. A 24, 321—324.

G. CROZAZ, R. WALKER, and D. WOOLUM (1971), Nuclear track studies of dynamic surface processes on the moon and the constancy of solar activity. Proc. Second Lunar Science Conf. Vol. 3, 2543—2558.

E. N. DUESLER and K. N. RAYMOND (1971), Conformational effects of intermolecular interactions. The structure of tris-(ethylene diamine) cobalt (III) monohydrogen phosphate nonohydrate. Inorg. Chem. 10, 1486—1492.

E. N. ELISEEV (1958), New data on the crystal structure of olivine. Kristallografiya 3, 167—175 [Russian]; Soviet Physics—Crystallogr. 3, 163—170.

L. W. FINGER (1967), Determination of cation distribution by least squares refinement of single-crystal x-ray data. Carnegie Institution Year Book 67, Ann. Report Geophysic. Lab., 216—217.

L. W. FINGER (1969/1970), Fe/Mg ordering in olivines. Carnegie Institution Year Book 69, Ann. Report Geophysic. Lab., 302—305.

L. W. FINGER (1971), Fe/Mg ordering in an olivine: a comparison of x-ray and Mössbauer results. Geol. Soc. Amer. abstracts 3, 310.

R. L. FLEISCHER, E. L. HAINES, H. R. HART, JR., R. T. WOODS, and G. M. COMSTOCK (1970), The particle track record of the Sea of Tranquillity. Proc. Apollo 11 Lunar Science Conf., Geochim. Cosmochim. Acta, Suppl. 1, Vol. 3, 2103—2120.

R. L. FLEISCHER, H. R. HART, JR., G. M. COMSTOCK, and A. O. EVWARAYE (1971), The particle track record of the Ocean of Storms. Proc. Second Lunar Science Conf., Vol. 3, 2559—2568.

S. GHOSE (1962), The nature of Mg^{+2}—Fe^{+2} distribution in some ferromagnesian silicate minerals. Amer. Mineral. 47, 388—394.

K. HANKE (1963), Verfeinerung der Kristallstruktur des Fayalits von Bad Harzburg. Neues Jahrb. Mineral., Monatsh. 192—194.

K. HANKE und J. ZEMANN (1963), Verfeinerung der Kirstallstruktur von Olivin. Naturwissenschaften 3, 91—92.

I. C. JAHANBAGLOO (1969), X-ray diffraction study of olivine solid solution series. Amer. Mineral. 54, 246—250.

J. L. JAMBOR and C. H. SMITH (1964), Olivine composition determination with small diameter x-ray powder cameras. Mineral. Mag. 33, 730—741.

H. ONKEN (1965), Verfeinerung der Kristallstruktur von Monticellit. Tschermak's Mineral. Petrogr. Mitt. 10, 34—44.

P. B. PRICE and D. O'SULLIVAN (1970), Lunar erosion rate and solar flare paleontology. Proc. Apollo 11 Lunar Science Conf. Geochim. Cosmochim. Acta Suppl. 1, Vol. 3, 2351—2359.

K. N. RAYMOND (1972), The application of constraints to derivatives in least-squares refinement. Acta Crystallogr. A 28, 163—166.

D. VIRGO, S. S. HAFNER and D. WARBURTON (1971), Cation distribution studies in clinopyroxenes, olivines and feldspars using Mössbauer spectroscopy of ^{57}Fe. Second Lunar Conf. Houston. [Unpublished proceedings].

H. S. YODER and T. G. SAHAMA (1957), Olivine x-ray determinative curve. Amer. Mineral. 42, 475—490.

W. H. ZACHARIASEN (1968), TeMe: Experimental tests of the general formula for the integrated intensity of a real crystal. Acta Crystallogr. A 24, 212